RESSALVA

Atendendo solicitação da autora, o texto completo deste documento será disponibilizado somente a partir de 18/06/2026.

SÃO PAULO STATE UNIVERISTY
Graduate Program in Mechanical Engineering
Campus Bauru

Camila Albertin Xavier da Silva

Dynamic Behavior of Finite Mono-Coupled Periodic Structures with Variable Cross-Section and Coupled Resonators

Bauru
2024

Camila Albertin Xavier da Silva

Dynamic Behavior of Finite Mono-Coupled Periodic Structures with Variable Cross-Section and Coupled Resonators

Thesis presented to the Graduate Program in Mechanical Engineering as part of the requirements for obtaining the title of Doctor in Mechanical Engineering from the Faculty of Engineering, São Paulo State University (UNESP), Campus Bauru.

Concentration area: Modeling and Design of Mechanical Systems.

Supervisor: Prof. Dr. Paulo J. Paupitz Gonçalves

Bauru
2024

S586d

Silva, Camila Albertin Xavier da

Dynamic Behavior of Finite Mono-Coupled Periodic Structures with Variable Cross-Section and Coupled Resonators / Camila Albertin Xavier da Silva. -- Bauru, 2024

120 p. : il., tabs.

Tese (doutorado) - Universidade Estadual Paulista (UNESP), Faculdade de Engenharia, Bauru

Orientador: Paulo José Paupitz Gonçalves

1. Periodic Structures. 2. Symmetrical / Asymmetrical Structure. 3. Super-attenuation / Multi-frequency bands. 4. Dynamic Vibration Absorbers. 5. Metastructure. I. Título.

Sistema de geração automática de fichas catalográficas da Unesp. Dados fornecidos pelo autor(a).

ATA DA DEFESA PÚBLICA DA TESE DE DOUTORADO DE CAMILA ALBERTIN XAVIER DA SILVA, DISCENTE DO PROGRAMA DE PÓS-GRADUAÇÃO EM ENGENHARIA MECÂNICA, DA FACULDADE DE ENGENHARIA - CÂMPUS DE BAURU.

Aos 18 dias do mês de dezembro do ano de 2024, às 9h, por meio de Videoconferência, realizou-se a defesa de TESE DE DOUTORADO de CAMILA ALBERTIN XAVIER DA SILVA, intitulada **Dynamic Behavior of Finite Mono-Coupled Periodic Structures with Variable Cross-Section and Coupled Resonators**. A Comissão Examinadora foi constituída pelos seguintes membros: Prof. Dr. PAULO JOSÉ PAUPITZ GONÇALVES (Orientador(a) - Participação Virtual) do(a) Departamento de Engenharia Mecânica / Universidade Estadual Paulista Unesp Faculdade de Engenharia Câmpus Bauru, Prof. Dr. FABRICIO CESAR LOBATO DE ALMEIDA (Participação Virtual) do(a) Departamento de Engenharia Mecânica / Universidade Estadual Paulista (Unesp) - Faculdade de Engenharia - Câmpus Bauru , Prof. Dr. FABIO MAZZARIOL SANTICIOLLI (Participação Virtual) do(a) Departamento de Engenharia Mecânica / Universidade Estadual Paulista, Prof. Dr. JOSÉ MARIA CAMPOS DOS SANTOS (Participação Virtual) do(a) Departamento de Mecânica Computacional / Universidade Estadual de Campinas - UNICAMP, Prof. Dr. RODRIGO BORGES SANTOS (Participação Virtual) do(a) Engenharia Mecânica / Universidade Federal da Grande Dourados. Após a exposição pela doutoranda e arguição pelos membros da Comissão Examinadora que participaram do ato, de forma presencial e/ou virtual, a discente recebeu o conceito final:_____APROVADA_____. Nada mais havendo, foi lavrada a presente ata, que após lida e aprovada, foi assinada pelo(a) Presidente(a) da Comissão Examinadora.

Prof. Dr. PAULO JOSÉ PAUPITZ GONÇALVES

Documento assinado digitalmente
PAULO JOSE PAUPITZ GONCALVES
Data: 19/12/2024 08:35:15-0300
Verifique em https://validar.iti.gov.br

In memory of my Mother, Mafalda Albertin Xavier da Silva.

ACKNOWLEDGEMENTS

This study was funded by the Coordination for the Improvement of Higher Education Personnel (CAPES), process number 88887.487924/2020-00, and the National Council for Scientific and Technological Development (CNPq), process number 384685/2024-2, for which I am deeply grateful. I also extend my gratitude to the ENVIBRO research group, funded by the São Paulo Research Foundation (FAPESP), for their invaluable support and contributions.

I would like to express my heartfelt thanks to the following:

UNESP, for providing an enriching environment that fostered my academic growth and development.

My supervisor, Paulo, whose guidance, patience, and encouragement have been instrumental in shaping both my academic journey and personal growth. I am deeply thankful for his belief in my potential and in the significance of this research.

Fabricio Lobato de Almeida, for their insightful feedback and constructive suggestions throughout my research years.

Professor Michael J. Brennan, for his teachings and contributions to my doctoral studies.

My family: Umberto and Mafalda (in loving memory), my sisters Franciellen and Amanda, my brother Umberto, and my stepmother Fátima, for their unwavering love and support.

My partner, André, whose love, support, and patience have been fundamental throughout this journey. I am also grateful to his parents, Milton and Evanice, for their encouragement and care.

My nephews, Maria, Francisco, and Noah, who brought light and joy during challenging times.

My friends and colleagues at UNESP, for their friendship, collaboration, and support along the way.

Finally, I offer my deepest gratitude to God and Mother Thrice Admirable for blessing me with this achievement and guiding me throughout my life.

“If you want to find the secrets of the universe, think in terms of energy, frequency, and vibration”.

Nikola Tesla

ABSTRACT

The interest in periodic structures has grown significantly in recent years, driven by their ability to efficiently manipulate waves, making them a promising solution for various applications in modern engineering systems. These structures are notable for their capacity to reduce vibrations within specific frequency ranges, with widespread applications in acoustic insulation in the aerospace sector and vibration control in civil structures. Recently, the metastructures, which consist of the integration of vibration absorbers into periodic structures, have been investigated as a means to expand the frequency ranges where vibration attenuation occurs. This study focuses on analyzing the dynamic behavior of finite mono-coupled periodic structures composed of rods with catenoidal, exponential, and conical shapes. To model these rods, their receptance and dynamic stiffness matrices are determined. The transfer matrix method is employed to derive the global properties of the structure based on the transmissibility of a single unit cell. The influence of the structure's geometry is analyzed by considering symmetric and asymmetric cells. It was observed that when the cells are composed of rods of the same length, asymmetric configurations exhibit greater wave attenuation, albeit limited to higher frequency ranges. The introduction of dynamic vibration absorbers into symmetric cells was investigated to create super-attenuation bands and multiple frequency attenuation bands. To validate the proposed methodology, experimental tests were conducted on a structure composed of conical rods, both in the absence and presence of dynamic vibration absorbers. The experimental results showed good agreement with theoretical predictions, reinforcing the effectiveness of the developed approach.

Keywords: Periodic Structures; Symmetrical / Asymmetrical Structure; Super -attenuation / Multi-frequency bands; Dynamic Vibration Absorbers; Metastructure.

RESUMO

O interesse por estruturas periódicas tem crescido significativamente nos últimos anos, impulsionado por sua capacidade de manipular ondas de maneira eficiente, o que as torna uma solução promissora para diversas aplicações em sistemas de engenharia modernos. Essas estruturas destacam-se por sua habilidade de reduzir vibrações em faixas de frequência específicas, sendo amplamente aplicadas em isolamento acústico no setor aeroespacial e no controle de vibrações em estruturas civis. Recentemente, as metaestruturas, que consistem na integração de absorvedores de vibração em estruturas periódicas, têm sido investigadas como uma forma de ampliar as faixas de frequência onde ocorre a atenuação vibracional. Este trabalho tem como foco a análise do comportamento dinâmico de estruturas periódicas monoacopladas finitas, compostas por barras com geometrias catenoidal, exponencial e cônica. Para modelar essas barras, são determinadas suas matrizes de receptância e rigidez dinâmica. O método da matriz de transferência é empregado para derivar as propriedades globais da estrutura a partir da transmissibilidade de uma única célula unitária. A influência da geometria da estrutura é analisada considerando células simétricas e assimétricas. Observou-se que, quando as células são formadas por barras de mesmo comprimento, as configurações assimétricas apresentam maior atenuação de ondas, embora restrita a faixas de frequência mais elevadas. A introdução de absorvedores dinâmicos de vibração em células simétricas foi investigada, visando à criação de bandas de superatenuação e a formação de múltiplas bandas de frequência atenuadas. Para validar a metodologia proposta, foram realizados ensaios experimentais em uma estrutura composta por barras cônicas, tanto na ausência quanto na presença de absorvedores dinâmicos de vibração. Os resultados experimentais demonstraram boa concordância com as previsões teóricas, reforçando a eficácia da abordagem desenvolvida.

Palavras-chave: Estruturas Periódicas; Estrutura Simétrica / Assimétrica, Super banda de atenuação / Bandas multifrequenciais; Absorvedores Dinâmicos de Vibração; Metaestruturas.

LIST OF FIGURES

Figure 1 – Illustrations of periodic structures: (a) unidimensional; (b) two-dimensional (c) three-dimensional. ______ 24

Figure 2 – Examples of passive, active and semiactive periodic structures: (a) geometric discontinuity; (b) material discontinuity; (c) active piezoelectric patches; (d) active shape memory inserts. ______ 25

Figure 3 – Periodic structure with a coupled resonator: (a) schematic representation of the single cell (b) experimental test of the single cell. ______ 27

Figure 4 – Illustration of the use of an isolation mechanism using a periodic foundation: (a) representation of the replacement of the traditional solid foundation by a periodic foundation; (b) Highlighting of the attenuation zone in the seismic response of the structure with the periodic foundation. ______ 28

Figure 5 – Schematic of the application of locally resonant metamaterials in an aircraft panel to enhance sound transmission loss: (a) Acoustic fuselage demonstrator at Airbus and schematic interior; (b) Metamaterial configuration with an example of a unit cell; (c) Representation and photograph of the resonator used in the metamaterial; (d) Dispersion diagram highlighting the stop band. ______ 28

Figure 6 – Schematicof the application of periodic structures in offshore platforms: (a) the periodic pipeline structure (b) offshore platform truss structure model. ______ 29

Figure 7 – Finite mono-coupled periodic structure with different cell arrangements. U_L represents the amplitude of displacement on the left-hand side, and U_R represents the amplitude of the displacement on the right-hand side. ______ 30

Figure 8 – Sets of cells formed by stepped rods: (a) and (b) symmetric cells; (c) and (d) asymmetric cells. All cells have length 2l. ______ 30

Figure 9 – Different configurations of a single cell for: (a) and (b) catenoidal symmetric cells; (c) and (d) catenoidal asymmetric cells; (e) and (f) exponential symmetric cells; (g)

and (h) exponential asymmetric cells; (i) and (j) conical symmetric cells; (k) and (l) conical asymmetric cells. All cells have length 2l and each segment of the cell has length l. __ 31

Figure 10 – Second subsets of asymmetric cells: (a) and (b) catenoidal asymmetric cells; (c) and (d) exponential asymmetric cells; (e) and (f) conical asymmetric cells. All cells have length 2l. ____ 32

Figure 11 – Representation of symmetric cell with length $2l$ with addition of dynamic vibration absorber attached at its center. Parameters of absorber: stiffness s_a, mass m_a and loss factor η_a. ____ 33

Figure 12 – Illustration of a portion of a rod: (a) undergoing axial deformation; (b) free-body diagram. ____ 37

Figure 13 – Illustration of a rod with a uniform cross-sectional area. ____ 39

Figure 14 - Illustration of a rod of variable cross-sectional area. ____ 41

Figure 15 – Rod with catenoidal varying cross-sectional area. ____ 42

Figure 16 – Rod with exponentially varying cross-sectional area. ____ 44

Figure 17 – Rod with conically varying cross-sectional area. ____ 45

Figure 18 – Comparison of transmissibilites responses of the rods with variable cross section: (a) Displacement transmissibility; (b) Point receptance (dB ref. 1m/N); (c) Transfer receptance (dB ref. 1m/N). ____ 49

Figure 19 – General mono-coupled structure comprising N periodic cells, highlighting a single cell n. The displacement amplitudes within the single cell are represented by $U_L^{[n]}$ on the left-hand side and $U_R^{[n]}$ on the right-hand side. The excitation force amplitudes in the single cell are denoted as $F_L^{[n]}$ on the left-hand side and $F_R^{[n]}$ on the right-hand side. ____ 52

Figure 20 – A single cell composed of two elements. ____ 54

Figure 21 – Periodic structure composed N cells where the cell is composed of two elements. 54

Figure 22 - Displacement transmissibility of a periodic structure with: (a) symmetric cells; (b) asymmetric cells with periodicity l; (c) asymmetric cells with periodicity $2l$. The black squares indicated the minimum transmissibility within the frequency band. 63

Figure 23 – Minimum of transmissibility within the lowest attenuation frequency band as a function of number of cells for symmetric and asymmetric cells. 64

Figure 24 – Deflections shapes for symmetrical and asymmetrical structures excited at the frequency of the minimum transmissibility within frequency band. 65

Figure 25 - Displacement transmissibility of periodic structures with asymmetric cells: (a) periodicity l; (b) periodicity $2l$. 66

Figure 26- Deflections shapes for an asymmetric structure with different orientations: (a) Excitation force at thinner left end; (b) Excitation force at the thicker left end. 67

Figure 27 - Displacement transmissibility of a periodic cell with different values of βl: (a) symmetric cell; (b) asymmetric cell; the red circles give the attenuation band limits and the black square gives the minimum transmissibility within these frequency bands. 68

Figure 28 - Stop/attenuation band as a function of the parameter βl: (a) and (b) Frequency limits of the attenuation/stop-band and the frequency defining the minimum attenuation for different βl values; (c) and (d) Minimum of transmissibility as a function of the βl. 69

Figure 29 – Comparison of the exponential and stepped rod transmissibilities (a) Displacement transmissibility of a periodic structure with symmetric cells; (b) Minimum of transmissibility within the lowest attenuation frequency band as a function of number of cells. 71

Figure 30 - Comparison of the exponential and stepped rod transmissibilities (a) Displacement transmissibility of a periodic structure with asymmetric cells; (b) Minimum

of transmissibility within the lowest attenuation frequency band as a function of number of cells. ________ 72

Figure 31 - Displacement transmissibility of a periodic structure with asymmetric cells. ________ 73

Figure 32 – General mono-coupled structure comprising N periodic cells, highlighting a single cell n composed of two exponential-shaped rods with an additional dynamic vibration absorber attached at its center. The parameters of the absorber are illustrated: stiffness (s_a), mass (m_a) and loss factor (η_a). The displacement amplitudes within the single cell are represented by $U_L^{[n]}$ on the left-hand side and $U_R^{[n]}$ on the right-hand side. The excitation force amplitudes in the single cell are denoted as $F_L^{[n]}$ on the left-hand side and $F_R^{[n]}$ on the right-hand side. The matrix $\mathbf{T}_{cell}$ represents the transfer matrix of the cell, which is composed of the matrices for rods C (matrix $\mathbf{T}_C$) and c (matrix $\mathbf{T}_c$) as well as the absorber (matrix $\mathbf{T}_{att}$). ________ 76

Figure 33 – Numerical simulation responses with the addition of the dynamic vibration absorber to the symmetric cell: (a) Displacement transmissibilites; (b) Point receptances; (c) Transfer receptances; the orange area provides the range of super attenuation band (SAB), the green area provides the stop band due to the Bragg scattering effect (BE) and the yellow area provides the range of local resonance effect (LRE); the red circles provide the stop-band limits of the structure without dynamic vibration absorber; black squares give the minimum transmissibilities within the frequency bands in figure (a-ii). ________ 80

Figure 34 - Frequency bands formed by the local resonance effect (LRE) and the Bragg effect (BE) are shown as γ is varied. The super-attenuation band is highlighted in $\gamma = 1$. The shaded areas represent the BE and LRE regions, while the red dashed lines indicate the boundaries of the frequency bands. p_1, p_2 and p_3 correspond to the peaks in the transmissibility response, while T_1 refers to the trough of the transmissibility response, which occurs at the natural frequency of the absorber. ________ 81

Figure 35 - Numerical simulation responses with the addition of the dynamic vibration absorber to the periodic structure: (a) Comparison of maximum attenuation within frequency bands about the number of cells; blue line without dynamic vibration absorber

and orange line with dynamic vibration absorber; (b) Displacement transmissibility of a periodic structure of symmetric cells with dynamic vibration absorber; orange line N = 1 cell; gray line N = 5 cells; the red dashed lines provide the super attenuation band limits; black squares give the minimum transmissibilities within the frequency band. ______ 82

Figure 36 - Frequency bands as a function of the parameter βl for symmetric cell (a) without the DVA; (b) with the DVA ($\upsilon = 0.3$). Minimum transmissibility as a function of the parameter βl for symmetric cell (c) without the DVA; (d) with the DVA. _______ 84

Figure 37 - Single symmetric cells composed by exponential-shaped rods (a) without DVA (b) with n_a rainbow-shaped dynamic vibration absorbers. ______________________ 85

Figure 38 - Displacement transmissibility of the single symmetric cells without DVA (blue line) and with rainbow-shaped absorbers (orange line): (a) with a decrease in mass $\Delta = -0.03$ (b) with no variation in mass $\Delta = 0$ (c) with an increase in mass $\Delta = 0.03$. The red dashed lines provide the frequency band limits. ______________________________ 88

Figure 39 - Schematic representation of the experimental setup, highlighting the data acquisition system, the placement of accelerometers at the ends of a cell, and the laptop used for recording and processing the experimental data. Additionally, two photographs showcasing the symmetric and asymmetric cells utilized in the experiments. _______ 91

Figure 40 - Comparison of experimental results with theoretical predictions using the model described in Section 4. (a) Transmissibility of a single symmetric cell, (b) Transmissibility of a single asymmetric cell (periodicity l). (c) Point receptance of a single symmetric cell, (d) Point receptance of a single asymmetric cell, (e) Transfer receptance of a single symmetric cell, (f) Transfer receptance of a single asymmetric cell. ______ 92

Figure 41 - Schematic of the experimental set-up. Highlighting the acquisition system, position of the accelerometers at the ends of a cell, the impact hammer and the laptop used to record and process the experimental data. Photograph shows the symmetric cell with DVA used in the experiments. ____ 93

Figure 42 - Illustration of dynamic vibration absorber. The screws and nuts act as the mass of the absorber. ____ 94

Figure 43 - Comparison of experimental results with theoretical predictions using the model described in Section 5.2 (a) Displacement transmissibility; (b) Point receptance (c) Transfer receptance. ____ 96

Figure 44 - Comparison of experimental results with theoretical predictions with dynamic vibration absorber and without dynamic vibration absorber. ____ 97

Figure 45 - Comparison of experimental results with theoretical predictions using the model described in Section 5.3: (ai-ii) Displacement transmissibility (bi-ii) Point receptances; (c-ii) Transfer receptances; the yellow area provides the range of local resonance effect (LRE) of theorical preditions; the green area provides the range of Bragg scattering effect (BE) of theorical predictions; grey line: experiment results, orange line: theoretical prediction. ____ 100

Figure C.1 – Comparison of the stop-bands of finite structures with the bandgaps of infinite structures (a) displacement transmissibility; (b) wave dispersion (real part of Λ); (c) wavenumber; red circles provide the stop-band/attenuation band limits.................115

Figure D.1 - Schematic representation of the roving excitation method, highlighting the nodes excited in the structure and the accelerometer positioned at the left end of a cell (point 17). Additionally, two photographs are provided showcasing the symmetric and asymmetric cells used in the experiments. 116

Figure D.2 - Complex Mode Indicator Function (CMIF) and mode shapes of the asymmetric cell..118

Figure D.3 - Complex Mode Indicator Function (CMIF) and mode shapes of the symmetric cell. 119

LIST OF TABLES

Table 1 – Receptance matrices of the rods with variable cross-sectional area. ________ 50

Table 2 – Dynamic stiffness matrices of the rods with variable cross-sectional area.__ 51

Table 3 - Transfer matrices of the rod elements. All rods have length l. ____________ 55

Table 4 - Equation of transmissibility $T_r = U_R^{[2]} / U_L^{[1]}$, for a single cell. All cells have length $2l$. ______ 59

Table 5 - Equation of transmissibility $T_r = U_R^{[2]} / U_L^{[1]}$, for a single cell. All cells have length $2l$. ______ 61

Table 6 - Values of the attenuation bandwidth for symmetric and asymmetric cells and the minimum transmissibility. ______ 72

Table 7 - Equation of transmissibility $T_r = U_R^{[2]} / U_L^{[1]}$, for a single cells with a dynamic vibration absorber (DVA) coupled at the central point of the cell. All cells have length $2l$. ______ 78

Table 8 - Parameters of the dynamic vibration absorber.______ 79

Table 9 - Values of the attenuation bandwidth and the minimum transmissibility for symmetric cells without DVA and with DVA. ______ 83

Table 10 - Parameters of the rainbow-shaped absorber.______ 86

Table 11 - Parameters of the dynamic vibration absorber.______ 95

Table 12 - Parameters of the dynamic vibration absorber used in the experimental procedure.______ 98

Table 13 - Parameters of the rainbow-shaped absorber used in the experimental procedure. ______ 99

Table D.1 - AutoMAC between modes to itself (asymmetric cell)................................ 117

Table D.2 - AutoMAC between modes to itself (symmetric cell)................................. 118

LIST OF ABBREVIATIONS AND ACRONYMS

AutoMac	Modal Assurance Criterion
BE	Bragg Scattering Effect
CMIF	Complex Mode Indicator Function
DSM	Dynamic Stiffness Method
DOF	Degree of Freedom
DVA	Dynamic Vibration Absorber
EMA	Experimental Modal Analysis
FEM	Finite Element Method
FRFs	Frequency Response Functions
LRE	Local Resonance Effect
SVD	Singular Value Decomposition

LIST OF SYMBOLS

Designation	Explanation
Latin symbols	
A	Constant cross-section area
A_L	Cross-section area at left-side end
A_R	Cross-section area at right-side end
$A(x)$	Variable cross-section area as a function of the position x
a_1, a_2	Constants for the uniform rod general solution
b_1, b_2	Constants for the catenoidal shaped rod general solution
c_0	Wave velocity for a rod with uniform cross-section area
c_1, c_2	Constants for the exponential shaped rod general solution
D_{att}	Dynamic stiffness of an attached vibration absorber
$D_{11}, D_{12}, D_{21}, D_{22}$	Elements of the dynamic stiffness matrix
d_1, d_2	Constants for the conical shaped rod general solution
E	Young's modulus of the rod
E_a, E_c	Young's modulus of the of the dynamic vibration absorber used in the experimental procedure
e_1, e_2	Constants for the Cayley-Hamilton Theorem
F_L	Amplitude of the excitation force at left end side
F_R	Amplitude excitation force at right end side
J_q	Bessel functions of the first kind of order q
k	Wavenumber for catenoidal shaped rods
$\hat{k}$	Wavenumber for exponential shaped rods
k_c	Wavenumber of the single cell
k_a	Longitudinal wavenumber of the rod calculated for the undamped natural frequency of the vibration absorber
k_0	Wavenumber of a rod with a uniform cross-section
l	Length of the rod

l_{cell}	Length of the single cell
m	Mass of the cell
m_a	Mass of the dynamic vibration absorber
m_n	Mass of the nut which composed the dynamic vibration absorber in the experimental procedure
m_s	Mass of the screw which composed the dynamic vibration absorber in the experimental procedure
m_1	Mass of the primary absorber
N	Number of cells
n_a	Number of absorbers
p	Constant of Bessel's equation
p_1, p_2, p_3	Peaks in the transmissibility response
q	Order of the Bessel functions
r_c	Radius of one of the parts that composes the dynamic vibration absorber in the experimental procedure
r_L	Radius of the left side end of structure
$R_{11}, R_{12}, R_{21}, R_{22}$	Elements of the receptance matrix
s_a	Stiffness of dynamic vibration absorber
s_1	Stiffness of the primary absorber
U_L	Amplitude of the longitudinal displacement at left end side
U_R	Amplitude of the longitudinal displacement at right end side
u	Amplitude of the longitudinal displacement along the axial direction
$\mathbf{T}$, $\mathbf{T}_{cell}$	Transfer matrix of a single cell
$\mathbf{T}_{att}$	Transfer matrix of a vibration absorber
T_1	Trough of the transmissibility response
$T_{11}, T_{12}, T_{21}, T_{22}$	Elements of the receptance matrix
t_a	Thickness of one of the parts that composes the dynamic vibration absorber in the experimental procedure
t	Time

x_L	Parameter that defines the shape of the cross-sectional for conical shaped rods
w_a	Width of one of the parts that composes the dynamic vibration absorber in the experimental procedure
Y_q	Bessel functions of the second kind of order q

Designation	Explanation
Greek symbols	
α	Parameter that defines the shape of the cross-sectional for catenoidal shaped rods
β	Parameter that defines the shape of the cross-sectional for exponential shaped rods
δ	Ratio of the cross-sectional area of the stepped rod
γ	Frequency ratio
Δ	Constant mass variation
ε	Longitudinal strain along the axial direction
η	Loss factor of the rod
η_a	Loss factor of the dynamic vibration absorber used in the experimental procedure
Λ	Eigenvalue of the transfer matrix
λ_0	Wavelength of rod with uniform cross-section
μ	Floquet exponent
ρ	Mass density of the rod
ρ_a	Mass density of the dynamic vibration absorber used in the experimental procedure
σ	Longitudinal stress along the axial direction
υ	Mass ratio
φ	Constant of Bessel's equation
ω	Circular frequency
ω_1	Natural frequency of the primary absorber

CONTENTS

1 INTRODUCTION 22
1.1 Motivation 22
1.2 Literature Review 23
1.2.1 Periodic Structures – Definition 23
1.2.2 Periodic Structures - Historical Background 25
1.3 Problem Statement 29
1.4 Objectives 33
1.5 Contributions to Knowledge 34
1.6 Thesis Structure 34
2 LONGITUDINAL VIBRATIONS IN RODS 36
2.1 Governing equations for axial deformation in rods 36
2.2 Rod with uniform cross-section 38
2.3 Rods of variable cross-section 41
2.3.1 Rod with catenoidal varying cross-sectional area 41
2.3.2 Rod with exponentially varying cross-sectional area 43
2.2.3 Rod with conically varying cross-sectional area 45
2.4 Displacement transmissibility of the rods with variable cross-sectional areas 47
2.5 Chapter Remarks 49
3 MODELING A PERIODIC STRUCTURE 52
3.1 The transfer matrix method 52
3.1.1 Transfer matrices of the rod elements 54
3.2 The Cayley-Hamilton theorem 56
3.2.1 Displacement transmissibility of the cells 58
3.3 Chapter Remarks 61
4 NUMERICAL SIMULATIONS FOR A FINITE PERIODIC STRUCTURE 62
4.1 Dynamic behavior for a finite periodic structure composed of rods with variation cross-section areas 62
4.1.1 The effect of parameter βl on transmissibility 67
4.2 Comparison with Stepped Rods 70
4.3 Chapter Remarks 73

5 SIMULATION FOR SYMMETRIC CELLS WITH THE ADDITION OF THE DYNAMIC VIBRATION ABSORBER ____ 75

5.1 Displacement transmissibility for cells with the addition of the dynamic vibration absorber 75

5.2 Formation of the super-attenuation band 78

5.3 Formation of multi-frequential bands 84

5.4 Chapter Remarks 89

6 EXPERIMENTAL VALIDATIONS ____ 90

6.1 Symmetric and asymmetric cells 90

6.2 Addition of the dynamic vibration absorber 93

6.2.1 Super - attenuation band 94

6.2.2 Multi-frequential bands 98

6.3 Chapter Remarks 101

7 CONCLUSIONS ____ 102

7.1 Scientific contribution 103

7.2 Future work suggestions 104

8 REFERENCES ____ 106

APPENDIX A – SOLUTION TO BESSEL DIFFERENTIAL EQUATION ____ 111

APPENDIX B – SOLUTION TO THE EQUATION OF MOTION IN SPACE DOMAIN OF THE ROD WITH CONICALLY VARYING CROSS-SECTION AREAS ____ 112

APPENDIX C – FLOQUET-BLOCH THEOREM AND THE DEFINITION OF STOP-BANDS ____ 113

APPENDIX D – EXPERIMENTAL MODAL ANALYSIS (EMA) ____ 116

1 INTRODUCTION

This chapter provides a brief motivation and a review of the literature on periodic structures, which form the foundation of this work. Additionally, the problem statement and objectives are outlined. Finally, the structure of the thesis report is presented.

1.1 Motivation

For several reasons, vibration can be considered an unwanted phenomenon in industrial systems and processes. Excessive vibration in vehicles, machines, or equipment can cause physical and mental discomfort to occupants or operators, and cause damage and premature failure to structures, machines, and devices (HUANG; GRIFFIN, 2014; LI; HUANG, 2018). When intense and continuous, vibration can lead the machine or equipment to material fatigue, and consequently to mechanical failure (LU *et al.*, 2023; WATBAN KHALID FAHMI; REZA KASHYZADEH; GHORBANI, 2022). These situations make vibration attenuation have an important role in the mechanical design stage, in which it becomes essential to apply vibration control techniques to resolve the presence of unwanted vibration, ensuring structural integrity and mechanical performance.

In recent decades, different vibration control techniques have been studied, known as passive, semi-active, or active. Among these techniques, the use of passive metamaterials has been highlighted. Passive metamaterials are periodic structures that exhibit periodicity based on geometric, material discontinuities, or the addition of resonators distributed in the structure. Due to this periodicity, these structures have the particular characteristic of forming frequency bands where the vibrational wave does not propagate, known as bandgaps (LIU; HUSSEIN, 2012). In this way, passive metamaterials become a useful alternative to suppress vibrations without the necessity for active vibration control (SANTOS *et al.*, 2023).

Several studies have been dedicated to reducing the propagation of vibration within a specific frequency range using such periodic systems. Recent research seeks to observe the behavior of the frequency band in relation to the geometry of periodic structures, as in the case of mono-coupled structures composed of stepped rod cells, which present satisfactory results in the attenuation of longitudinal waves mentioned in the use of stepped rods is the sudden change in the cross-sectional area, which can cause stress concentration at discontinuities (CARNEIRO *et al.*, 2021; SANTOS *et al.*, 2023). One of the methods to reduce stress concentration is avoid corner, using smooth geometries, for instance, as explored in the work of Taylor *et al.* (2011). Periodic structures composed of rods with smooth and variable cross-sectional areas could potentially solve the problem of stress concentrations and also guarantee the Bragg stop-band, due to the variation in the cross-sectional area.

Some advances still seen in the design of periodic structures to reduce the transmission of vibrations explore the use of vibration absorbers to broaden the frequency ranges in which frequency bands occur or to create multi-frequency bandgaps in lower frequency ranges. Cleante *et al.* (2022) explored the local resonance of the dynamic vibration absorber in periodic structures in order to obtain an ultra-wide frequency band, known as the super stop-band. Hao *et al.* (2019) concluded that the positions of local resonance and Bragg bandgaps can be adjusted by changing the natural frequency of the vibration absorbers. Mao, Zhang and Fan (2023) analyzed the vibration bandgaps in a non-uniform beam with periodically continuous variable cross-sections with coupled absorbers and concluded that disordered absorbers can broaden the bandgaps and generate various local resonance bandgaps.

Given this context, this research aims to investigate the dynamic behavior of finite mono-coupled periodic structures with variable cross-section and coupled resonators. The objective is to analyze how the variation in cross-sectional geometry and the inclusion of resonators influence the formation and characteristics of vibration attenuation bands. The study involves analytical modeling, numerical simulations, and experimental validations to optimize the performance of these periodic structures. By integrating variable geometries and coupled resonators, this research contributes to the advancement of vibration control strategies, providing effective solutions for engineering applications

1.2 Literature Review

1.2.1 Periodic Structures – Definition

Periodic structures are arrangements of repeating structural units, commonly referred to as cells, which are uniformly interconnected. These structures can exhibit periodicity in one, two, or three dimensions, as illustrated in Figure 1. In mono-coupled configurations, wave transmission occurs predominantly in one direction, while multi-coupled structures exhibit multiple degrees of freedom between cells, allowing wave propagation in multiple directions.

Figure 1 – Illustrations of periodic structures: (a) unidimensional; (b) two-dimensional (c) three-dimensional.

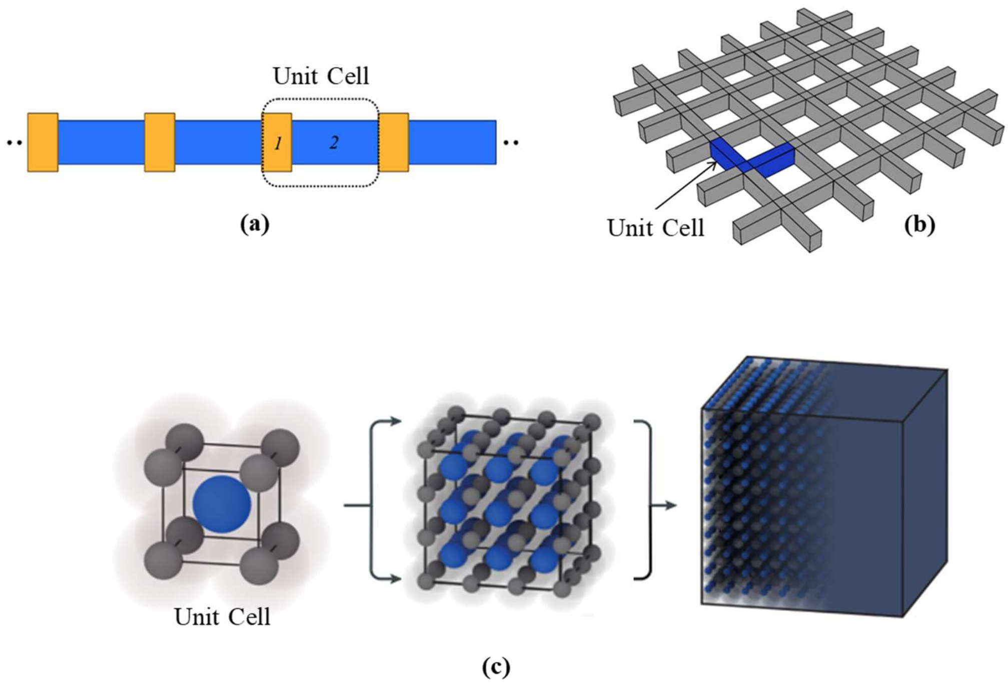

Source: Adapted from Cenedese, Belloni and Braghini (2021), Yang *et al*. (2022) and Kadic *et al*. (2019).

Periodic structures are broadly classified as passive, active, and semiactive. Passive structures rely on inherent properties like geometry or material discontinuities, while active structures incorporate components such as piezoelectric patches to adapt their dynamic response by directly injecting energy into the system. Semiactive structures, on the other hand, utilize controllable elements—such as shape memory alloys (SMAs) used to modify stiffness or damping— which adjust parameters without adding mechanical energy to the system. Figure 2 illustrates examples of all three classifications.

Due to periodicity shown in Figure 2, periodic structures exhibit unique dynamic properties. The Bragg scattering effect is one of the phenomena presents in such systems. This phenomenon occurs when the wavelength becomes comparable to the length of the structural cells, resulting in frequency regions where waves do not propagate. Such regions are known as “bandgaps” (BRILLOUIN, 1946).

Therefore, periodic structures are often called mechanical filters to the propagation of waves. The frequency bands where waves propagate along periodic structures are called “pass bands” and the specific frequency bands where waves do not propagate (for infinite periodic structure) are called “bandgaps”, or “stop-bands” (for finite periodic structure), where the waves are atenuated . In passive periodic structures, the spectral width and location of these bands are fixed, whereas in active periodic structures the bands are adjustable in relation to the vibration response (BAZ, 2019). It is important to distinguish between the concepts of bandgaps and attenuation bands. Bandgaps refer to frequency ranges in infinite structures where waves do not propagate freely within a waveguide, while attenuation bands are associated with frequency ranges in finite periodic structures where waves are attenuated (DA SILVA *et al*., 2025). According to the investigation carried out by Carneiro *et al*. (2021), in finite mono-coupled periodic structures, when the cells are symmetric, the attenuation band occurs in the same frequency range as the bandgap in an infinite structure. In the case of asymmetric cells, the attenuation band tends to be wider for a smaller number of cells, but decreases until it becomes approximately equivalent to the bandgap of an infinite asymmetric structure (DOMADIYA *et al*., 2016; HVATOV; SOROKIN, 2015).

Figure 2 – Examples of passive, active and semiactive periodic structures: (a) geometric discontinuity; (b) material discontinuity; (c) active piezoelectric patches; (d) active shape memory inserts.

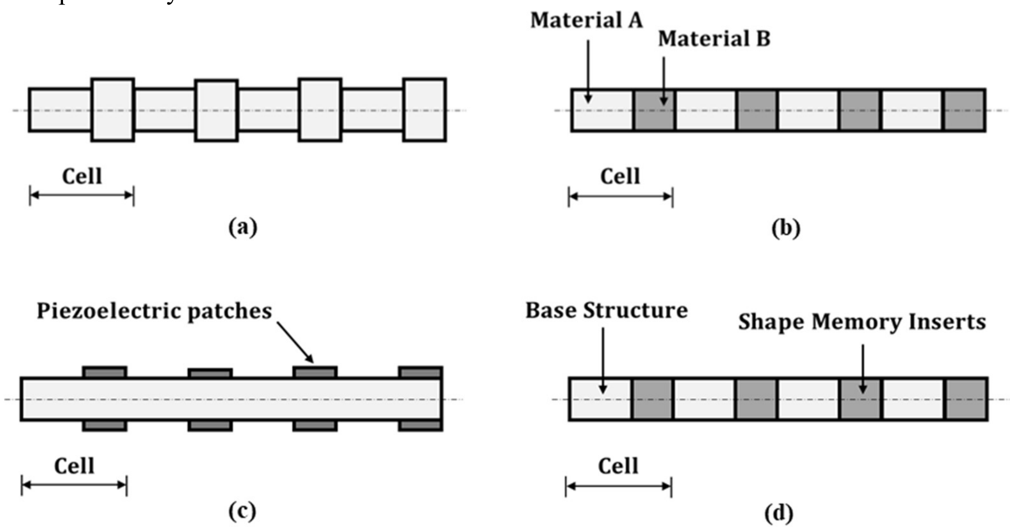

Source: Adapted from Baz (2019).

1.2.2 Periodic Structures - Historical Background

The study of periodic structures began with the work of Brillouin (1946), who investigated the theoretical foundations of wave propagation in periodic systems. In this work, Brillouin (1946) approached how the periodicity of a structure could influence wave transmission, establishing the basis for the concept of bandgaps, which characterize frequency regions where waves do not propagate. This idea aroused significant interest within the scientific community, particularly due to the potential for controlling vibrations and waves in mechanical structures.

Since then, the interest in periodic structures has grown exponentially, especially because of their ability to manipulate mechanical and vibrational waves. One of the main phenomena associated with these structures is Bragg scattering, which plays a crucial role in the formation of bandgaps. This phenomenon occurs when incident waves encounter periodic interfaces, where the geometric or material periodicity of the structure causes destructive interference in propagating waves, blocking them in specific frequency ranges (BRILLOUIN, 1946).

The concept of bandgaps, introduced by Brillouin (1946), was expanded upon by subsequent research investigating how structural characteristics, such as cell size and geometry, affect the position and width of these bands. Mead (1970 and 1971) was one of the pioneers in relating structural periodicity to the dynamic behavior of waves, providing a theoretical foundation for developing structures capable of attenuating vibrations in specific frequency ranges. Simultaneously, Cremer and Heckl (1973) contributed to the characterization of vibrational behavior in periodic systems with various structural configurations.

In more recent years, advancements in analytical and numerical methods, such as the transfer matrix method and Cayley-Hamilton theorem, have enabled more detailed modeling of Bragg scattering in finite mono-coupled structures. These methods have been applied to accurately predict the dynamic behavior of structures, particularly in analyzing the displacement transmissibility at the structure's ends, as extensively explored by Gonçalves, Brennan and Cleante (2021). Additionally, the use of Floquet-Bloch theorem is widely employed in the analysis of infinite periodic structures, allowing for accurate prediction of frequency bandgaps (HVATOV; SOROKIN, 2015).

The interaction between Bragg scattering and local resonators has become a significant topic in recent research. Studies such as those by Cenedese, Belloni and Braghin (2021) demonstrated that combining adjustable local resonators with periodic structures could result in broader and more effective bandgaps, enabling vibration control over more diverse frequency ranges. Raghavan and Phani (2013) investigated periodic resonators and coupled masses on a finite structural beam using receptance coupling methods and Bloch's theorem. Cleante *et al*. (2022) focused on studying the dynamic behavior of mono-coupled periodic structures with the addition of vibration absorbers, Figure 3 providing a detailed study on the influence of absorber parameters in achieving super-stop band.

Figure 3 – Periodic structure with a coupled resonator: (a) schematic representation of the single cell (b) experimental test of the single cell.

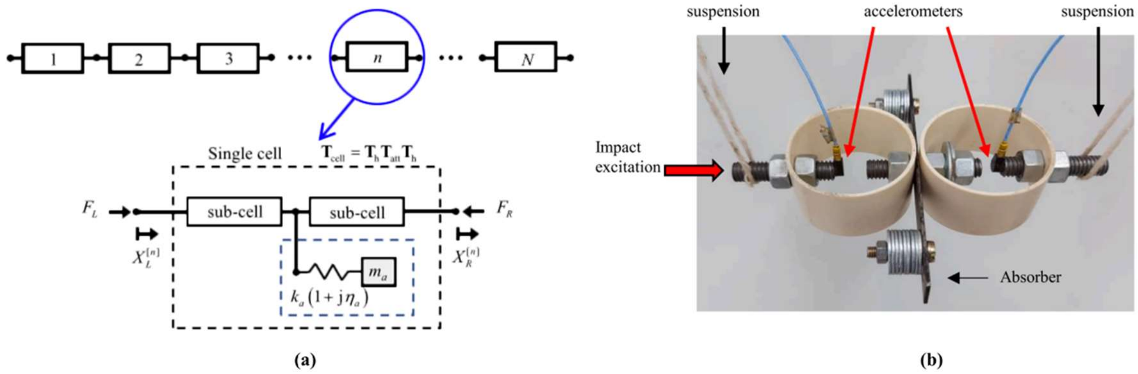

Source: Adapted from Cleante *et al*. (2022).

This integration paved the way for developing adjustable systems, such as adding smart materials to structures, including shape memory alloys and piezoelectrics, which opened new possibilities for designing active structures (LIU *et al*., 2024; SONG; SHEN, 2019; KUMBHAR *et al*., 2018).

In engineering applications, periodic structures have demonstrated great versatility in a wide range of uses due to their ability to manipulate mechanical waves and control vibrations. In civil engineering, the use periodic foundation are used for the control of seismic events and to serve as a vibration isolator, as shown in Figure 4 (CHENG *et al.*, 2020; CHENG; SHI, 2017; XIANG *et al.*, 2012; YAN *et al.*, 2015).

In aeronautical engineering, there are studies on the application of locally resonant metamaterials in the aircraft panel to improve sound insulation, according to Figure 5 (ALVES PIRES *et al*., 2022). There are also applications in aerospace engineering, where there is the development of metamaterials for applications in satellites (RAMACHANDRAN; FARUQUE; ISLAM, 2020).

Figure 4 – Illustration of the use of an isolation mechanism using a periodic foundation: (a) representation of the replacement of the traditional solid foundation by a periodic foundation; (b) Highlighting of the attenuation zone in the seismic response of the structure with the periodic foundation.

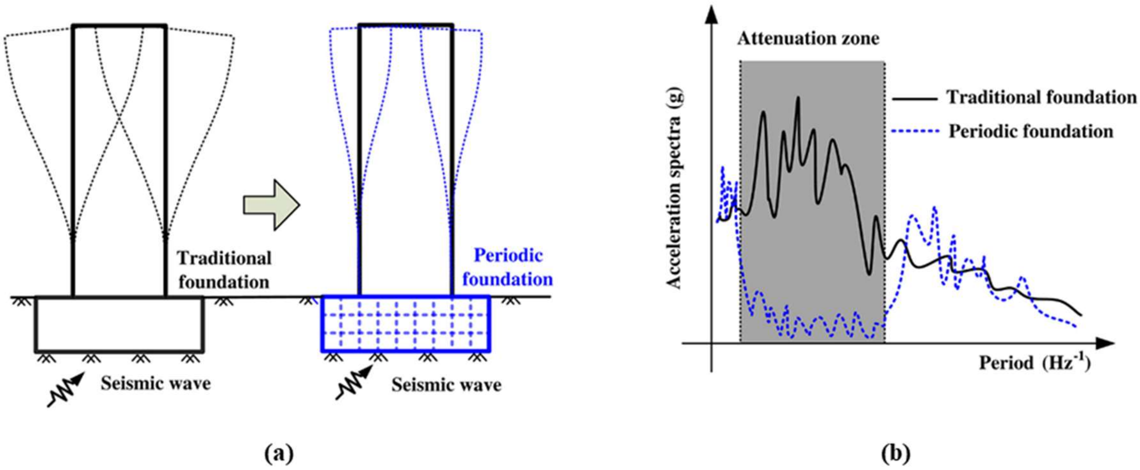

Source: Adapted from Cheng and Shi (2017).

Figure 5 – Schematic of the application of locally resonant metamaterials in an aircraft panel to enhance sound transmission loss: (a) Acoustic fuselage demonstrator at Airbus and schematic interior; (b) Metamaterial configuration with an example of a unit cell; (c) Representation and photograph of the resonator used in the metamaterial; (d) Dispersion diagram highlighting the stop band.

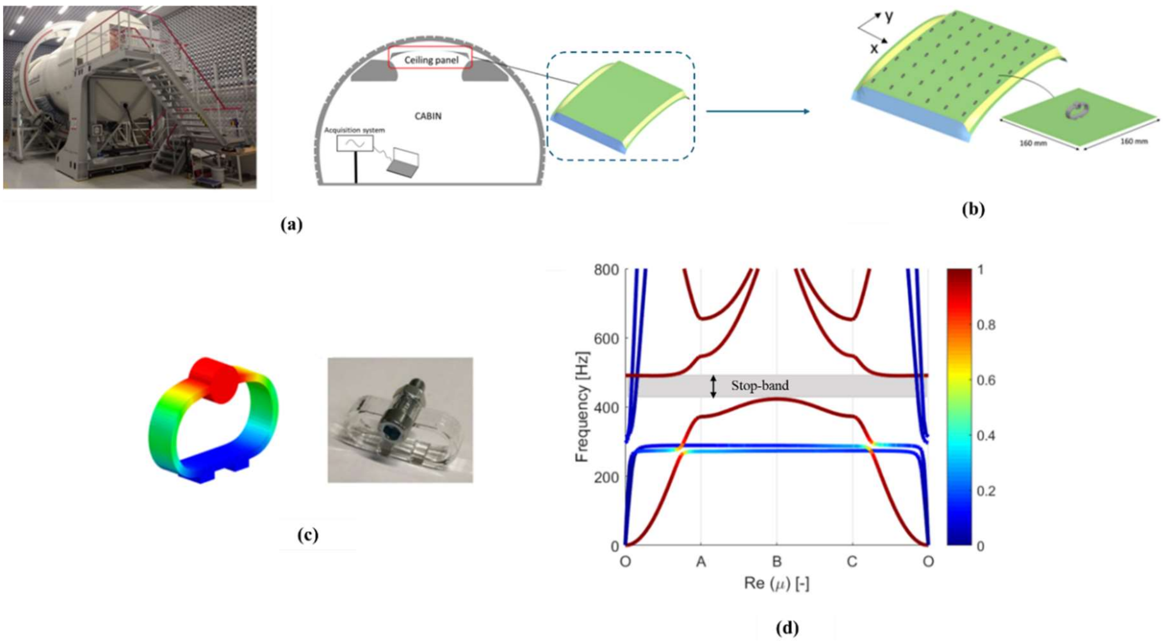

Source: Adapted from Alves Pires *et al*. (2022) .

In naval engineering, many studies are focused on the application of periodic structures on offshore platforms to realize the vibration control of the truss structure, as shown in Figure 6 (AZEVEDO VASCONCELOS *et al*., 2024; LAO *et al*., 2022; ZHAOWANG *et al*., 2020).

Figure 6 – Schematic of the application of periodic structures in offshore platforms: (a) the periodic pipeline structure (b) offshore platform truss structure model.

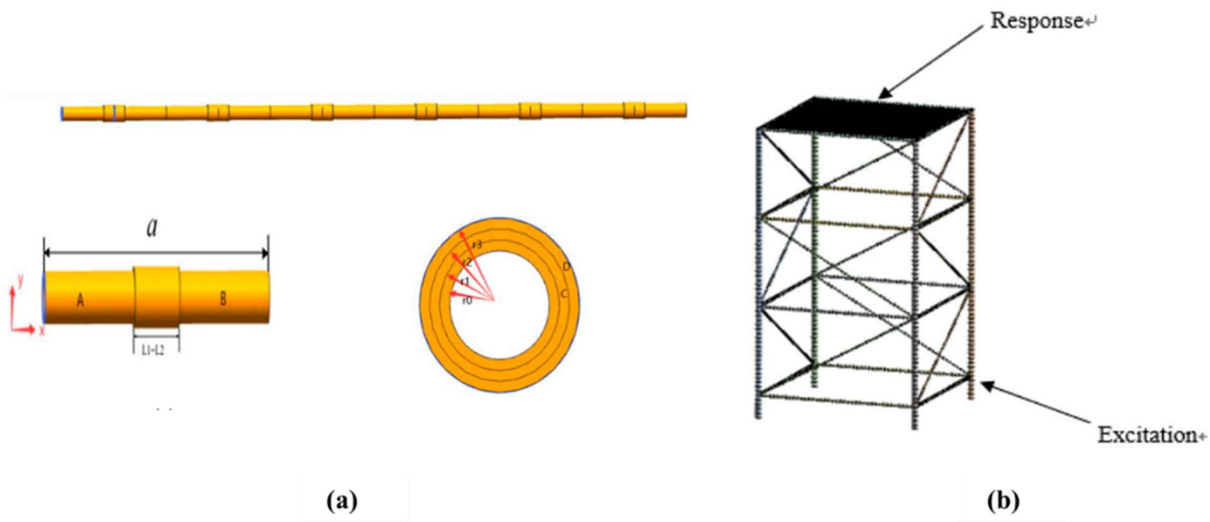

Source: Adapted from Lao *et al.* (2022) .

This overview demonstrates the ongoing impact of studying periodic structures, both in theory and practical applications, and their relevance in contemporary science and engineering.

1.3 Problem Statement

Since the use of periodic structures is a useful alternative to control the propagation of longitudinal vibration, the work aims to explore the use of finite mono-coupled periodic structures to obtain vibrational wave attenuation, through the evaluation of the displacement transmissibility response of the ends of the structure. Figure 7 exemplifies a periodic structure with geometric variation of the cross-sectional area, composed of N cells and exemplifies different arrangements of cells of which this structure can be composed.

Figure 7 – Finite mono-coupled periodic structure with different cell arrangements. U_L represents the amplitude of displacement on the left-hand side, and U_R represents the amplitude of the displacement on the right-hand side.

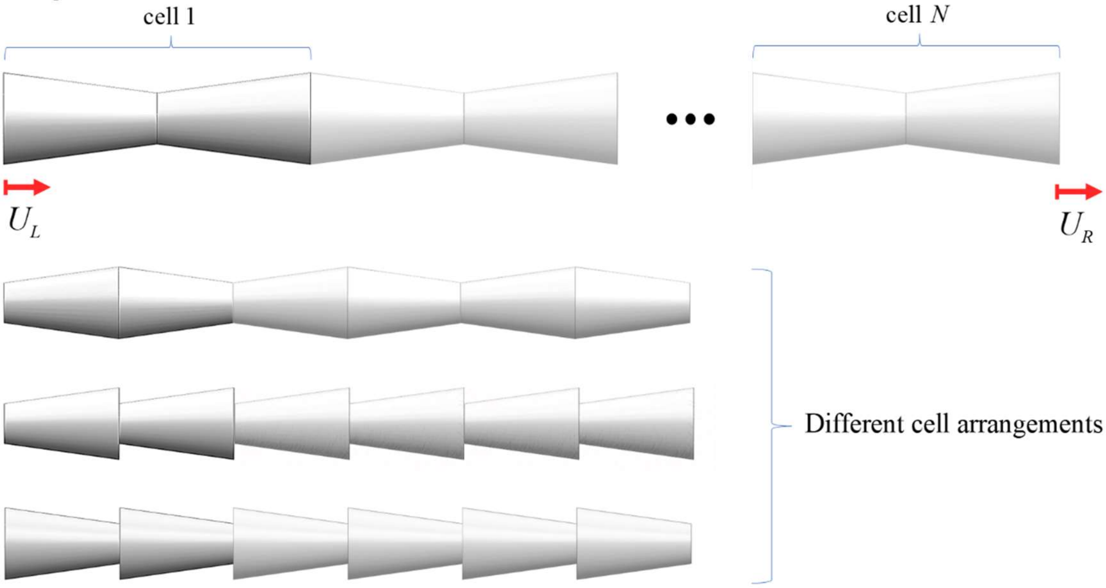

Source: Author own elaboration.

As mentioned previously, the sets of cells formed by stepped rods, shown in Figure 8, may present problems related to stress concentration at discontinuities, and a solution that can potentially solve this problem is the change to cells composed of rods with areas smooth and variable cross-sections. Given this, the work proposes a finite monocoupled periodic structure with new arrangements of periodic cells composed of rods that have variable cross-sectional areas, to guarantee the attenuation of longitudinal waves in the periodic structure through the formation of the Bragg stop-band.

Figure 8 – Sets of cells formed by stepped rods: (a) and (b) symmetric cells; (c) and (d) asymmetric cells. All cells have length 2*l*.

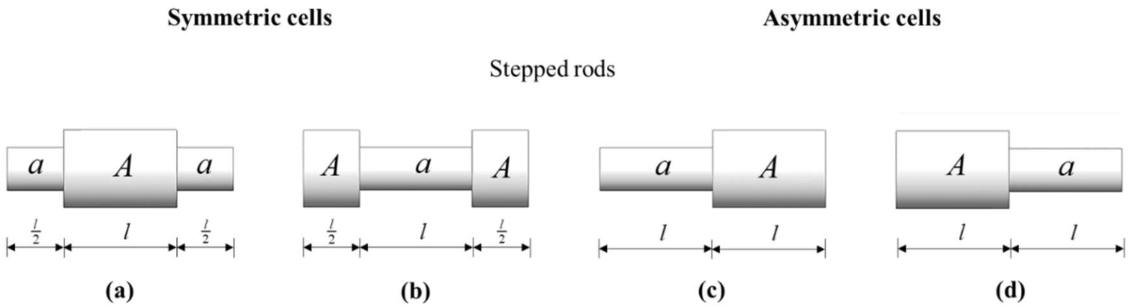

Source: Author own elaboration.

The sets of cells formed by rods with variable cross-sectional areas are shown in Figure 9. The cells are composed of two rods of the same length that have catenoidal, exponential, or conical shapes, and are divided into subsets of symmetric or asymmetric cells.

Figure 9 – Different configurations of a single cell for: (a) and (b) catenoidal symmetric cells; (c) and (d) catenoidal asymmetric cells; (e) and (f) exponential symmetric cells; (g) and (h) exponential asymmetric cells; (i) and (j) conical symmetric cells; (k) and (l) conical asymmetric cells. All cells have length $2l$ and each segment of the cell has length l.

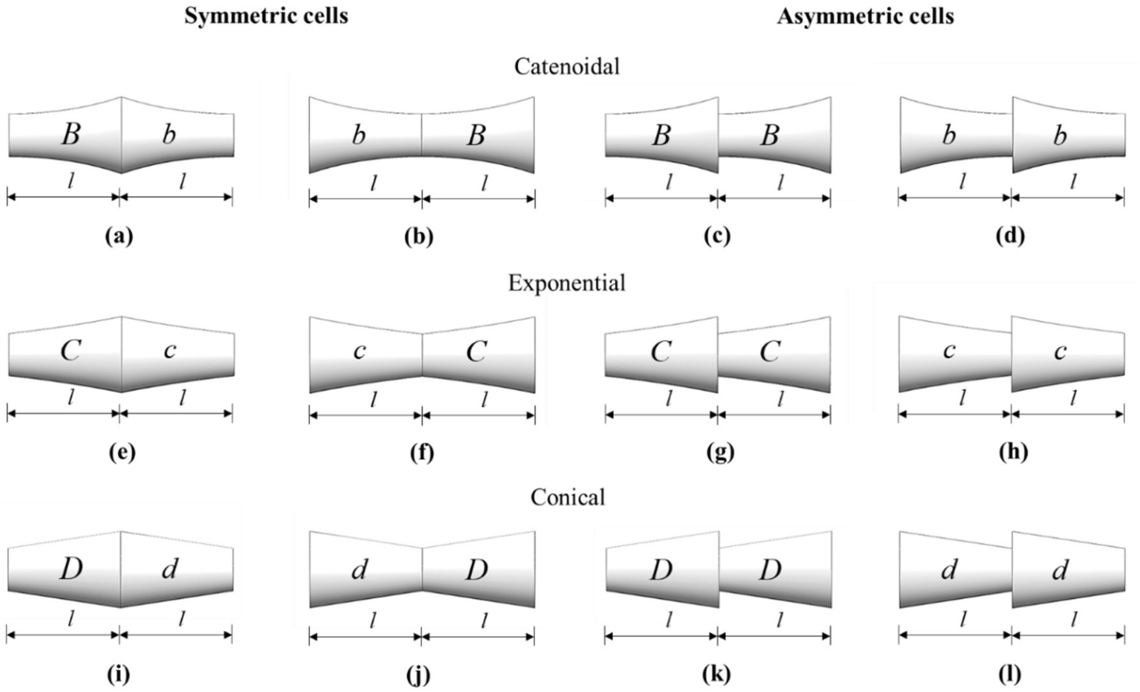

Source: Author own elaboration.

Since the asymmetric cell arrangements in Figure 9 present a sudden change in cross-section, a significant influence on the occurrence of attenuation band is expected, which may occur in different frequency ranges of the symmetric cells. Thus, the work addresses a second subset of asymmetric cells, which has the same cell length, but without a sudden change in the cross-sectional area of the cell.

Figure 10 – Second subsets of asymmetric cells: (a) and (b) catenoidal asymmetric cells; (c) and (d) exponential asymmetric cells; (e) and (f) conical asymmetric cells. All cells have length $2l$.

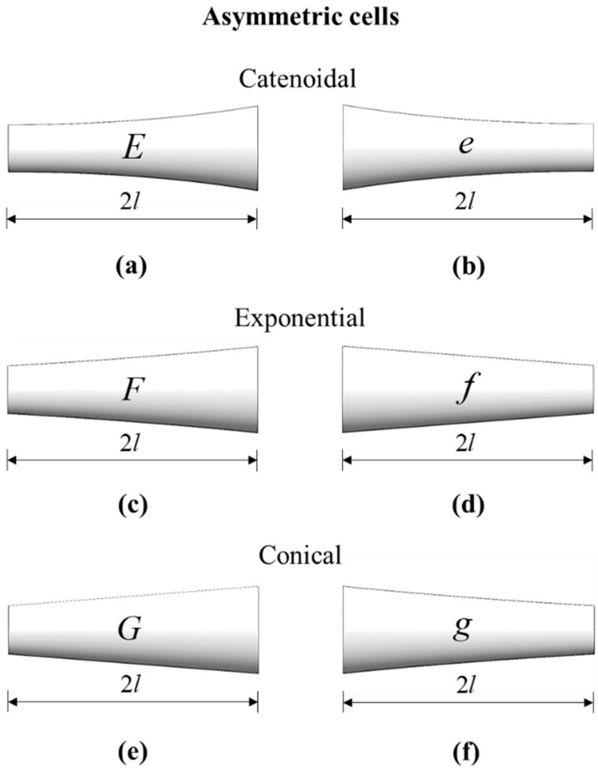

Source: Author own elaboration.

To analyze the propagation and attenuation of the longitudinal wave in the periodic structure, the work focuses on obtaining the response of the displacement transmissibility between the ends of the periodic structure (U_R/U_L). The displacement transmissibility allows visualization regions in which the frequency bands for wave attenuation occurred. Therefore, based on analytical equations of displacement transmissibility, the work aims to reduce vibration in specific frequency bands. To achieve this, the work is based on the method described by Gonçalves, Brennan and Cleante (2021), in which the displacement transmissibility of a single element can be used to estimate the dynamic response of a finite structure composed of N periodic cells. Therefore, to apply the proposed methodology, it is first necessary to model the system, for this purpose, the dynamic stiffness and receptance matrices of the rods that form the periodic structures are obtained. Next, the transfer matrix method is applied, and consequently, the analytical transmissibility equations of the cells that form the periodic structure are obtained.

To improve vibration attenuation, the work explores the addition of dynamic vibration absorbers in the symmetric cell, as shown in Figure 11, to obtain wider frequency ranges of attenuation, through the combination of the local resonance of the absorber and the Bragg stop-band or obtain multi-frequency attenuation bands from disordered local resonances.

Figure 11 – Representation of symmetric cell with length $2l$ with addition of dynamic vibration absorber attached at its center. Parameters of absorber: stiffness s_a, mass m_a and loss factor η_a.

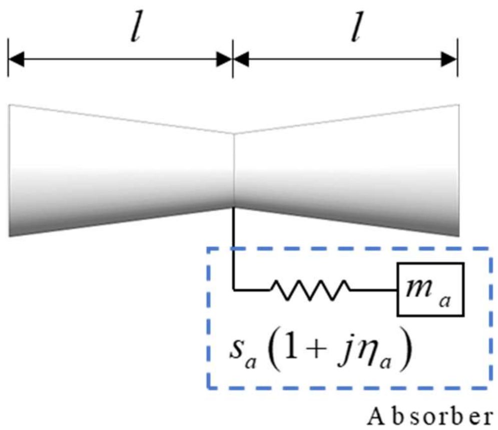

Source: Author own elaboration.

Experimental tests must be carried out to highlight and validate the results obtained in the proposed methodologies, emphasizing the effects obtained in attenuation bands.

1.4 Objectives

The main objective of this thesis is to analyze the dynamic behavior of finite mono-coupled periodic structures composed of rods with variable cross-sectional areas, focusing on the formation of stop-bands to achieve attenuation of longitudinal vibration waves. By incorporating dynamic vibration absorbers into the structure, the aim is to broaden the vibration attenuation bands or create attenuation bands at lower frequencies. The specific objectives are as follows:

1. To develop dynamic stiffness and receptance matrices for the rods with variable cross-sectional areas that constitute the periodic structure.
2. To derive analytical equations defining the transmissibility of a single cell.
3. To analyze the geometric effects regarding the composition of the structure by symmetric or asymmetric cells.

4. To analyze the dynamic effects of adding dynamic vibration absorbers to symmetric cells and compare these results with those of cells without absorbers.

5. To validate the results through experimental tests.

1.5 Contributions to Knowledge

This thesis makes several significant contributions to the field of vibration control:

1. Analytical Framework:

   This work develops a detailed analytical framework for modeling the dynamic behavior of finite mono-coupled periodic structures composed of rods with non-uniform cross-sectional areas. It provides analytical expressions for the transmissibility of individual cells, enabling efficient and accurate predictions of the dynamic response.

2. Geometrical Insights:

   The study advances the understanding of how different cell geometries (symmetric and asymmetric) affect vibration attenuation. It demonstrates that smoothly varying geometries, such as catenoidal, exponential, and conical bars, reduce stress concentrations while maintaining or enhancing the effectiveness of attenuation bands compared to stepped rods.

3. Coupling of Dynamic Vibration Absorbers:

   The thesis explores the coupling of dynamic absorbers in symmetric cells, showcasing their ability to create super-attenuation bands and multi-frequency attenuation bands. Rainbow-shaped absorbers are highlighted for their capacity to broaden the local resonance band, expanding the operational frequency range of periodic structures.

4. Experimental Validation:

   The methodology undergoes experimental validation, ensuring that theoretical predictions align with observed behavior. A series of controlled experiments confirm the accuracy of the analytical and numerical models, demonstrating the practical feasibility of the proposed structures and their effectiveness in vibration attenuation.

1.6 Thesis Structure

This thesis is divided into seven chapters. Chapter 1 introduces the study, providing motivation, a literature review on periodic structures, the problem statement, and the objectives of the work. Chapter 2 presents the modeling of the rods used to compose the periodic structures under study, including uniform rods and rods with catenoidal, exponential, and conical shapes. Chapter 3 describes the methodology for obtaining the analytical displacement responses of cell assemblies. Chapter 4 investigates the geometric parameters of the cells, focusing on symmetric and asymmetric configurations, based on the resulting stop-bands. Chapter 5 explores the addition of dynamic vibration absorbers to symmetric cells. Chapter 6 details the experimental tests, comparing the results with the analytical expressions derived in Chapters 4 and 5. Finally, Chapter 7 summarizes the conclusions of the thesis.

7 CONCLUSIONS

This thesis investigated the propagation of longitudinal waves in rods composed of cells with catenoidal, conical, and exponentially varying cross-sectional areas. In Chapter 2 , the structures were modeled in terms of receptance and dynamic stiffness matrices. Analytical equations for the displacement transmissibility of single cells were derived in Chapter 3 , using the transfer matrix method in combination with the Cayley-Hamilton theorem. These analytical equations provided the foundation for analyzing the dynamic behavior of finite mono-coupled periodic structures.

In Chapter 4, the dynamic behavior of periodic structures was investigated in terms of single-cell dynamics and periodicity effects. It was found that structures composed of rod elements with catenoidal, conical and exponentially varying cross-sectional areas present similar responses for displacement transmissibility. Regarding the periodicity of the cell, it was verified that asymmetric cells that present the same periodicity as symmetric cells, present results similar to symmetric cells. However, when rods of the same length are arranged in symmetric and asymmetric cells, both do not have the same periodicity length. It was found that for such a configuration, the correctly oriented asymmetric cells (the thinner end of the rod oriented towards the excitation source) have an attenuation band at higher frequencies compared to the symmetric structure. Additionally, the use of exponential-shaped rods was shown to provide satisfactory results for vibration attenuation while reducing stress concentrations compared to stepped rods.

Chapter 5 explored the integration of dynamic absorbers into periodic structures. The inclusion of these absorbers demonstrated the ability to create super-attenuation bands (ultra-wide attenuation bands) when tuned to the natural frequency of the structure. However, such attenuation bands occur at higher frequencies. As an alternative to overcome this challenge, the absorbers were tuned to frequencies lower than the natural frequency, resulting in the creation of multifrequency bands: one associated with the local resonance of the absorber and another related to the Bragg scattering effect. Nevertheless, the attenuation bands associated with local resonance are narrower compared to the Bragg bandwidth. To increase the bandwidth of the local resonance, a rainbow configuration of the absorbers was proposed, a strategy that proved effective in expanding the local resonance bandwidth, significantly enhancing the structure's capability for vibration control at lower frequency ranges.

The experimental validation was conducted in Chapter **6** to compare theoretical predictions with experimental results. The initial tests evaluated the responses of simple symmetric and asymmetric cells composed of rods with conical transverse variations. Although the rods exhibited bending modes, as discussed in Appendix E, these modes did not interfere with the formation of the frequency band.

Subsequently, dynamic absorbers were incorporated into the symmetric cells to achieve super-attenuation bands or attenuation bands at lower frequencies. Initially, a super-attenuation band was obtained, whose responses showed good agreement with theoretical predictions. Later, the absorber was adjusted to operate at lower frequencies, where it presented a high attenuation value, albeit within a narrow frequency range. To overcome this limitation, expand the local resonance bandwidth, the configuration of rainbow-shaped absorbers was experimentally implemented. The results demonstrated that rainbow-shaped absorbers are capable of broadening the bandwidth, although with a reduction in maximum attenuation. Thus, it is concluded that the experimental results corroborated theoretical predictions, confirming the effectiveness of the proposed methodology.

7.1 Scientific contribution

Parts of this research have been published in the literature, which can be cited:

1. DA SILVA, CAMILA ALBERTIN XAVIER; SOROKIN, VLADISLAV ; BRENNAN, MICHAEL JOHN ; GONÇALVES, PAULO JOSÉ PAUPITZ . The dynamic behaviour of a finite periodic structure comprising either symmetric or asymmetric exponential- and conical-shaped rods. JOURNAL OF SOUND AND VIBRATION, v. 595, p. 118741, 2025. https://doi.org/10.1016/j.jsv.2024.118741

2. DA SILVA, CAMILA ALBERTIN XAVIER; GONCALVES, P. J. P. . Periodic structures with exponentially varying cross-section areas. In: CILAMCE-PANACM-2021, 2021, Rio de Janeiro. Proceedings of the Ibero-Latin-American Congress on Computational Methods in Engineering. Belo Horizonte/MG: Associação Brasileira de Métodos Computacionais em Engenharia (ABMEC), 2021.

7.2 Future work suggestions

Based on the findings of this study, the following directions are suggested for future research:

- Modeling shear modes with the Rayleigh-Love theory:

Extend the current modeling approach to include shear deformation effects by applying the Rayleigh-Love theory. This would provide a more comprehensive understanding of the dynamic behavior of rods, especially for higher-frequency applications or cases where shear modes significantly influence the response.

- Exploration of bending effects:

Investigate the bending dynamics in the structural behavior, including bending vibrations and their interactions with other vibration modes. This study could enhance the understanding of the overall dynamic response and improve the design of structures for applications requiring precise vibration control or wave manipulation.

- Integration of Acoustic Black Holes into structures with exponential-shaped rods:

Explore the potential of exponential rods in the creation of Acoustic Black Holes leveraging geometric profiles to concentrate and dissipate vibrational energy. The inclusion of viscoelastic layers can enhance wave absorption, significantly reducing reflection and increasing vibration attenuation.

- Study of periodic structures with mixed periodicity (geometric and material):

Investigate the dynamic behavior of periodic structures that combine both geometric and material periodicity. This approach could lead to novel metamaterial designs with enhanced tunability and adaptive characteristics, broadening the range of applications in vibration control and wave manipulation.

- Development of more complex structures:

Based on the geometry studied in the thesis, to explore the construction of more complex structures using the modeled rods. This may involve assembling the rods into multidimensional frameworks or integrating them with additional structural elements in periodic systems. These structures can be tailored for specific dynamic behaviors, including enhanced vibration control and wave propagation management, for practical engineering applications.

8 REFERENCES

ALLEMANG, R. J.; BROWN, D. L. **A complete review of the complex mode indicator function (CMIF) with applications**. Proceedings of ISMA 2006: International Conference on Noise and Vibration Engineering, 2006.

ALVES PIRES, F.; WANDEL, M.; THOMAS, C.; DECKERS, E.; CLAEYS, C**. Improve sound transmission loss of an aircraft's lining panel by the use of locally resonant metamaterials**. 12th International Styrian Noise, Vibration & Harshness Congress: The European Automotive Noise Conference, 2022. Graz, Austria: SAE International, p. 1–11, 2022.

AYRES JR, F. **Theory and Problems of Matrices (Shaums's Outline Series).** New York: Shaum Publishing Co., 1962.

AZEVEDO VASCONCELOS, A. C.; VALIYA VALAPPIL, S.; SCHOTT, D.; JOVANOVA, J.; ARAGÓN, A. M. **A metamaterial-based interface for the structural resonance shielding of impact-driven offshore monopiles**. Engineering Structures, v. 300, 2024.

BANERJEE, J. R.; ANANTHAPUVIRAJAH, A.; PAPKOV, S. O. **Dynamic stiffness matrix of a conical bar using the Rayleigh-Love theory with applications**. European Journal of Mechanics, A/Solids, v. 83, 2020.

BAZ, A. M. S. **Vibration Control with Periodic Structures**. Active and passive vibration damping. 1. ed. Honoken: John Wiley & Sons Ltd, p. 523–588, 2019.

BOWMAN, F. **Introduction to Bessel Functions**. New York: Dover Publications Inc., 1958. 1–135 p.

BRILLOUIN, L. **Wave Propagation in Periodic Structures: Electric Filters and Crystal Lattices**. 1. ed. New York and London: McGraw-Hill Book Company Inc., p. 1–247, 1946.

CARNEIRO, J. P.; BRENNAN, M. J.; GONÇALVES, P. J. P.; CLEANTE, V. G.; BUENO, D. D.; SANTOS, R. B. **On the attenuation of vibration using a finite periodic array of rods comprised of either symmetric or asymmetric cells**. Journal of Sound and Vibration, v. 511, n. 116217, 2021.

CENEDESE, M.; BELLONI, E.; BRAGHIN, F. **Interaction of Bragg scattering band gaps and local resonators in mono-coupled periodic structures.** Journal of Applied Physics, 2021.

CHENG, Z. B.; SHI, Z F. **Composite periodic foundation and its application for seismic isolation**. Earthquake Engineering & Structural Dynamics, v. 47, n. 4, p. 925–944, 2017.

CHENG, Z.; SHI, Z.; PALERMO, A.; XIANG, H.; GUO, W.; MARZANI, A. **Seismic vibrations attenuation via damped layered periodic foundations.** Engineering Structures, v. 211, n. 110427, 2020.

CLEANTE, V. G.; BRENNAN, M. J.; GONÇALVES, P. J. P.; CARNEIRO, J. P. **On the formation of a super stop-band in finite mono-coupled periodic structures using an array of vibration absorbers: Controlling parameters and physical insight**. Mechanical Systems and Signal Processing, v. 180, 2022.

CRAIG, R. R.; ANDREW KURDILA, J. J. **Fundamentals of Structural Dynamics**. 2nd edition, 2006.

CREMER, L.; HECKL, M. **Structure-Borne Sound: Structural Vibrations and Sound Radiation at Audio Frequencies**. New York: Springer-Verlag Berlin Heidelberg , p. 1–528, 1973.

DA SILVA, C. A. X.; SOROKIN, V.; BRENNAN, M. J.; GONÇALVES, P. J. P. **The dynamic behaviour of a finite periodic structure comprising either symmetric or asymmetric exponential- and conical-shaped rods**. Journal of Sound and Vibration, v. 595, 2025.

DARCHE, M.; LOPEZ-CABALLERO, F.; TIE, B. **Modal analysis of waveguide for the study of frequency bandgaps of a bounded periodic medium**. Journal of Sound and Vibration, v. 572, 2024.

DOMADIYA, P. G.; MANCONI, E.; VANALI, M.; ANDERSEN, L. V; RICCI, A. **Numerical and experimental investigation of stop-bands in finite and infinite periodic one-dimensional structures**. Journal Vibration and Control, v. 22, n. 4, p. 920–931, 2016.

FAULKNER, M. G.; HONG, D. P. **Free vibrations of a mono-coupled periodic system.** Journal of Sound and Vibrarion. v. 99, p. 29-42, 1985.

GONÇALVES, P. J. P.; BRENNAN, M. J.; CLEANTE, V. G. **Predicting the stop-band behaviour of finite mono-coupled periodic structures from the transmissibility of a single element**. Mechanical Systems and Signal Processing, v. 154, 2021.

GRAFF, K. F. **Wave motion in elastic solids**. New York: Dover Publications, 1991.

GUPTA, A.; SHARMA, R.; THAKUR, A.; GULIA, P. **Metamaterial foundation for seismic wave attenuation for low and wide frequency band**. Scientific Reports, v. 13, n. 1, 2023.

HAN, J. B.; HONG, S. Y.; SONG, J. H.; KWON, H. W. **Vibrational energy flow models for the Rayleigh-Love and Rayleigh-Bishop rods**. Journal of Sound and Vibration, v. 333, n. 2, p. 520–540, 2014.

HAO, S.; WU, Z.; LI, F.; ZHANG, C. **Numerical and experimental investigations on the band-gap characteristics of metamaterial multi-span beams.** Physics Letters, Section A: General, Atomic and Solid State Physics, v. 383, n. 36, 2019.

HUANG, Y.; GRIFFIN, M. J. **The discomfort produced by noise and whole-body vertical vibration presented separately and in combination**. Ergonomics, v. 57, n. 11, p. 1724–1738, 2014.

HVATOV, A.; SOROKIN, S. **Free vibrations of finite periodic structures in pass- and stop-bands of the counterpart infinite waveguides**. Journal of Sound and Vibration, v. 347, p. 200–217, 2015.

KADIC, M.; MILTON, G. W.; VAN HECKE, M.; WEGENER, M. **3D metamaterials.** Nature Reviews Physics. Springer Nature, 2019.

KALKOWSKI, M. K.; MUGGLETON, J. M.; RUSTIGHI, E. **Wave propagation in rods with an exponentially varying cross-section - Modelling and experiments**. Journal of Physics: Conference Series, 1., 2016. Institute of Physics Publishing, v. 744, 2016.

KHOO, S. Y.; LIAN, Y. C.; ONG, Z. C.; ISMAIL, Z.; NOROOZI, S**. Feasibility study of performing experimental modal analysis with oblique impact testing using various oblique impact directions**. Alexandria Engineering Journal, v. 59, n. 1, p. 457–473, 2020.

KUMBHAR, S. B.; CHAVAN, S. P.; GAWADE, S. S. **Adaptive tuned vibration absorber based on magnetorheological elastomer-shape memory alloy composite**. Mechanical Systems and Signal Processing, v. 100, p. 208–223, 2018.

LAO, X.; YU, Y.; ZHANG, F.; YE, J.; XU, X.; XIA, Z. **Research on Locally Resonant Characteristics of Pipelines with Periodic Structure**. Micromachines, v. 13, n. 850, p. 1–14, 2022.

LI, D.; HUANG, Y. **The discomfort model of the micro commercial vehicles interior noise based on the sound quality analyses**. Applied Acoustics, v. 132, p. 223–231, 2018.

LIU, B.; CHEN, P.; ZHU, T.; WANG, Y. F. **Tunable bandgaps in an elastic meta-plate with shape memory alloy springs**. Extreme Mechanics Letters, v. 72, 2024.

LIU, L.; HUSSEIN, M. I. **Wave motion in periodic flexural beams and characterization of the transition between Bragg scattering and local resonance**. Journal of Applied Mechanics, Transactions ASME, v. 79, n. 1, 2012.

LIU, X.; ZHAO, Y.; ZHOU, W.; BANERJEE, J. R. **Dynamic stiffness method for exact longitudinal free vibration of rods and trusses using simple and advanced theories**. Applied Mathematical Modelling, v. 104, p. 401–420, 2022.

LU, H.; WANG, J.; LIAN, Y.; WEN, Z.; LIU, T.; YUE, Z. **Random vibration fatigue behavior of directionally solidified superalloy: Experiments and evaluation of life prediction methods**. International Journal of Fatigue, v. 175, 2023.

MAO, X.; ZHANG, L.; FAN, X. **Wave attenuation of a multi-span continuous beam with variable cross sections.** Acta Mechanica, v. 234, n. 4, p. 1451–1464, 1 abr. 2023.

MEAD, D. J. **Free wave propagation in periodically supported, infinite beams**. Journal of Sound and Vibration, v. 11, n. 2, p. 181–197, 1970.

MEAD, D. J. **Vibration Response and Wave Propagation in Periodic Structures**. Journal of Engineering for Industry , v. 93, n. 3, p. 783–792, 1971.

MEAD, D. J. **Wave propagation in continuous periodic structures: research contributions from Southampton**, Journal of Sound and Vibration, v. 90, n. 3, p. 495-524, 1996.

MEAD, D. J. **Passive Vibration Control.** 1st. ed. Wiley, 1999.

MENG, H.; CHRONOPOULOS, D.; FABRO, A. T.; ELMADIH, W.; MASKERY, I. **Rainbow metamaterials for broadband multi-frequency vibration attenuation: Numerical analysis and experimental validation**. Journal of Sound and Vibration, v. 465, 2020.

NIELSEN, R. B.; SOROKIN, S. V. **Periodicity effects of axial waves in elastic compound rods**. Journal of Sound and Vibration, v. 353, p. 135–149, 2015.

PU, X.; SHI, Z. **Surface-wave attenuation by periodic pile barriers in layered soils**. Construction and Building Materials, v. 180, p. 177–187, 2018.

RAGHAVAN, L.; PHANI, A. S. **Local resonance bandgaps in periodic media: Theory and experiment.** The Journal of the Acoustical Society of America, v. 134, n. 3, p. 1950–1959, 2013.

RAO, S. **Mechanical Vibrations**. 5th. ed. Pearson, 2010.

RAMACHANDRAN, T.; FARUQUE, M. R. I.; ISLAM, M. T. **A dual band left-handed metamaterial-enabled design for satellite applications**. Results in Physics, v. 16, 2020.

RUBIN, S. **Mechanical Immittance and Transmission-Matrix Concepts**. The Journal of the Acoustical Society of America, v. 41, p. 1171–1179, 1967.

SANTOS, R. B.; BERRES, G.; INMAN, D. J.; GONSALEZ-BUENO, C. G.; BUENO, D. D. **A practical approach to evaluate periodic rods composed of cells with geometric and material periodicity**. Journal of Sound and Vibration, v. 553, 2023.

SONG, Y.; SHEN, Y. **Shape memory metamaterials with adaptive bandgaps for ultra-wide frequency spectrum vibration control**. ASME 2019 International Mechanical Engineering Congress and Exposition. Salt Lake City, Utah, USA, 2019.

TAYLOR, D.; KELLY, A.; TOSO, M.; SUSMEL, L. **The variable-radius notch: Two new methods for reducing stress concentration**. Engineering Failure Analysis, v. 18, n. 3, p. 1009–1017, 2011.

TIMOSHENNKO, S.; GOODIER, J. N. **Theory of Elasticity**. McGraw-Hill Book Company, Inc., 1951.

WATBAN KHALID FAHMI, A. T.; REZA KASHYZADEH, K.; GHORBANI, S. **A comprehensive review on mechanical failures cause vibration in the gas turbine of combined cycle power plants**. Engineering Failure Analysis. Elsevier Ltd, 2022.

XIANG, H. J.; SHI, Z. F.; WANG, S. J.; MO, Y. L. **Periodic materials-based vibration attenuation in layered foundations: experimental validation**. Smart Materials and Structures, v. 21, n. 112003, p. 1–10, 2012.

YAN, Y.; CHENG, Z.; MENQ, F.; MO, Y. L.; TANG, Y.; SHI, Z. **Three dimensional periodic foundations for base seismic isolation. Smart Materials and Structures**, v. 24, n. 075006, p. 1–11, 2015.

YANG, B.; ZINE, A.; DROZ, C.; ICHCHOU, M. **Two-dimensional periodic structures modeling based on second strain gradient elasticity for a beam grid Two-dimensional periodic struc-tures modeling based on second strain gradient elasticity for a beam grid Two-dimensional periodic structures modeling based on second strain gradient elasticity for a beam grid**. International Journal of Mechanical Sciences, v. 222, p. 1–13, 2022.

ZHAOWANG, X.; XIANGXI, X.; FUYU, J.; ZONGYAO, W.; ZHIWEI, L.; RUI, C. **Study on vibration characteristics of periodic truss structure of offshore platform**. Advances in Mechanical Engineering, v. 12, n. 11, p. 1–7, 2020.

APPENDIX A – Solution to Bessel differential equation

This appendix presents the solution to Bessel differential equation. The Bessel differential equation is the linear second-order ordinary differential equation given by equation (A.1).

$$x^2 U'' + xU' + \left(x^2 - m^2\right)U\left(x\right) = 0 \tag{A.1}$$

where m is a real constant, called the order of the Bessel equation.

Bowman (1958) suggests a transformation of the Bessel Equation that satisfies $U\left(x\right) = x^p J_q\left(\chi x^\varphi\right)$, then

$$U''\left(x\right) - \frac{2p-1}{x}U' + \left(\chi^2\varphi^2 x^{2\varphi-2} + \frac{p^2 - q^2\varphi^2}{x^2}\right)U\left(x\right) = 0 \tag{A.2}$$

Therefore, the solution is given by equation (A.3).

$$U\left(x\right) = \begin{cases} x^p\left[d_1 J_q\left(\chi x^\varphi\right) + d_2 Y_q\left(\chi x^\varphi\right)\right] & \text{for integer, } q \\ x^p\left[d_1 J_q\left(\chi x^\varphi\right) + d_2 J_{-q}\left(\chi x^\varphi\right)\right] & \text{for nointeger, } q \end{cases} \tag{A.3}$$

where $J_q\left(x\right)$ and $Y_q\left(x\right)$ are the Bessel functions of the first and second kind, and d_1 and d_2 are arbitrary constants.

APPENDIX B – Solution to the equation of motion in space domain of the rod with conically varying cross-section areas

In this appendix are considered the rod with conically varying cross-section areas, its equation of motion, given by equation (32), and the solution to Bessel differential equations, according to Appendix A.

The equation of motion in the space domain of rod with conically varying cross-section areas, according to Graff (1991) is given by the Bessel differential equation, according to equation (32). From the transformation proposed by Bowman (1958), according to equation (A.2), the values of p, φ, χ and q are respectively

$$p=-\frac{1}{2}; \qquad \varphi=1; \qquad \chi=k_0; \qquad q=\frac{1}{2}$$

Therefore, the solution for equation (32) is the Bessel equation of half-order, according to equation (B.1)

$$U(x)=\frac{1}{\sqrt{x}}\left[d_1 J_{\frac{1}{2}}(k_0 x)+d_2 J_{-\frac{1}{2}}(k_0 x)\right] \tag{B.1}$$

According to the properties of the Bessel function, $J_{\frac{1}{2}}(x)$ and $J_{-\frac{1}{2}}(x)$ are obtained by expansions in power series, then

$$J_{\frac{1}{2}}(x)=\sqrt{\frac{2}{\pi x}}\sum_{n=0}^{\infty}\frac{(-1)^n}{(2n+1)!}x^{2n+1}=\sqrt{\frac{2}{\pi x}}\sin(x) \tag{B.2}$$

$$J_{-\frac{1}{2}}(x)=\sqrt{\frac{2}{\pi x}}\sum_{n=0}^{\infty}\frac{(-1)^n}{(2n)!}x^{2n}=\sqrt{\frac{2}{\pi x}}\cos(x) \tag{B.3}$$

Substituting the equations (B.2) and (B.3) in equation (B.1), the solution of equation (32) is given by

$$U(x)=\frac{1}{x}\left[d_1 \sin(k_0 x)+d_2 \cos(k_0 x)\right] \tag{B.4}$$

APPENDIX C – Floquet-Bloch theorem and the definition of stop-bands

In this appendix, the application of the Floquet-Bloch theorem in finite periodic systems and its relationship with the formation of stop-bands is discussed. The theorem is widely applied to infinite structures to calculate the dispersion properties of periodic structures and to estimate their wave modes and velocities (DARCHE; LOPEZ-CABALLERO; TIE, 2024; GUPTA *et al.*, 2023; PU; SHI, 2018).

With the transfer matrix of the unit cell well defined, the Floquet-Bloch theorem can be applied to relate the state vectors of the right and left faces of the periodic structure, where, ${q_R}^{[N]} = \Lambda\, {q_L}^{[1]}$, where Λ is the eigenvalue of the transfer matrix, given by.

$$\Lambda = e^{\mu} = e^{-i k_c l_{cell}} \tag{C.1}$$

where $i = \sqrt{-1}$, l_{cell} is the length of cell and k_c is the wavenumber of the cell, given by

$$k_c(\omega) = \frac{\ln(\Lambda(\omega))}{i\, l_{cell}} \tag{C.2}$$

where ω is the circular frequency.

In the context of periodic structures, the theorem allows defining frequency regions where wave propagation occurs, known as pass-bands. These occur when $|\Lambda| = 1$, where the wavenumber k_c is purely real, indicating that the wave propagates through the structure without attenuation. Frequency regions where waves do not propagated freely are known as bandagps. In these regions, $|\Lambda| \neq 1$, with k_c has an imaginary part, indicating that the wave is evanescent and decays exponentially (BRILLOUIN, 1946).

As mentioned, the theorem is widely used for infinite periodic structures, allowing the prediction of the frequencies at which stop-band will occur based on the dispersion curves. However, as discussed in Chapter 4, in structures with symmetric cells, the lower and upper limits of the stop-band do not change with an increasing number of cells. Thus, the lower and upper limits of the stop-band of a finite structure composed of symmetric cells are the same as those of the stop-band of an infinite structure. Therefore, for symmetric structures, the dispersion curves can be analyzed using the eigenvalues of the unit cell transfer matrix, and it is also possible to perform an analysis based on the wavenumber (NIELSEN; SOROKIN, 2015).

However, it was discussed in Chapter 4 that in asymmetric structures, as the number of cells increases, the attenuation band narrows until it reaches the lower and upper limits of the stop-band of an infinite structure. Thus, for asymmetric structures with a reduced number of cells, wavenumber dispersion curves would not be an option to predict the attenuation bands accurately.

Figure C.1 presents the analysis of the relationship between displacement transmissibility and the wave and wavenumber dispersion curves to determine the stop-bands. For cells composed of exponential-shaped rods, $k_c = \hat{k}$, and $l_{cell} = 2l$.

Figure C.1 – Comparison of the stop-bands of finite structures with the bandgaps of infinite structures (a) displacement transmissibility; (b) wave dispersion (real part of Λ); (c) wavenumber; red circles provide the stop-band/attenuation band limits.

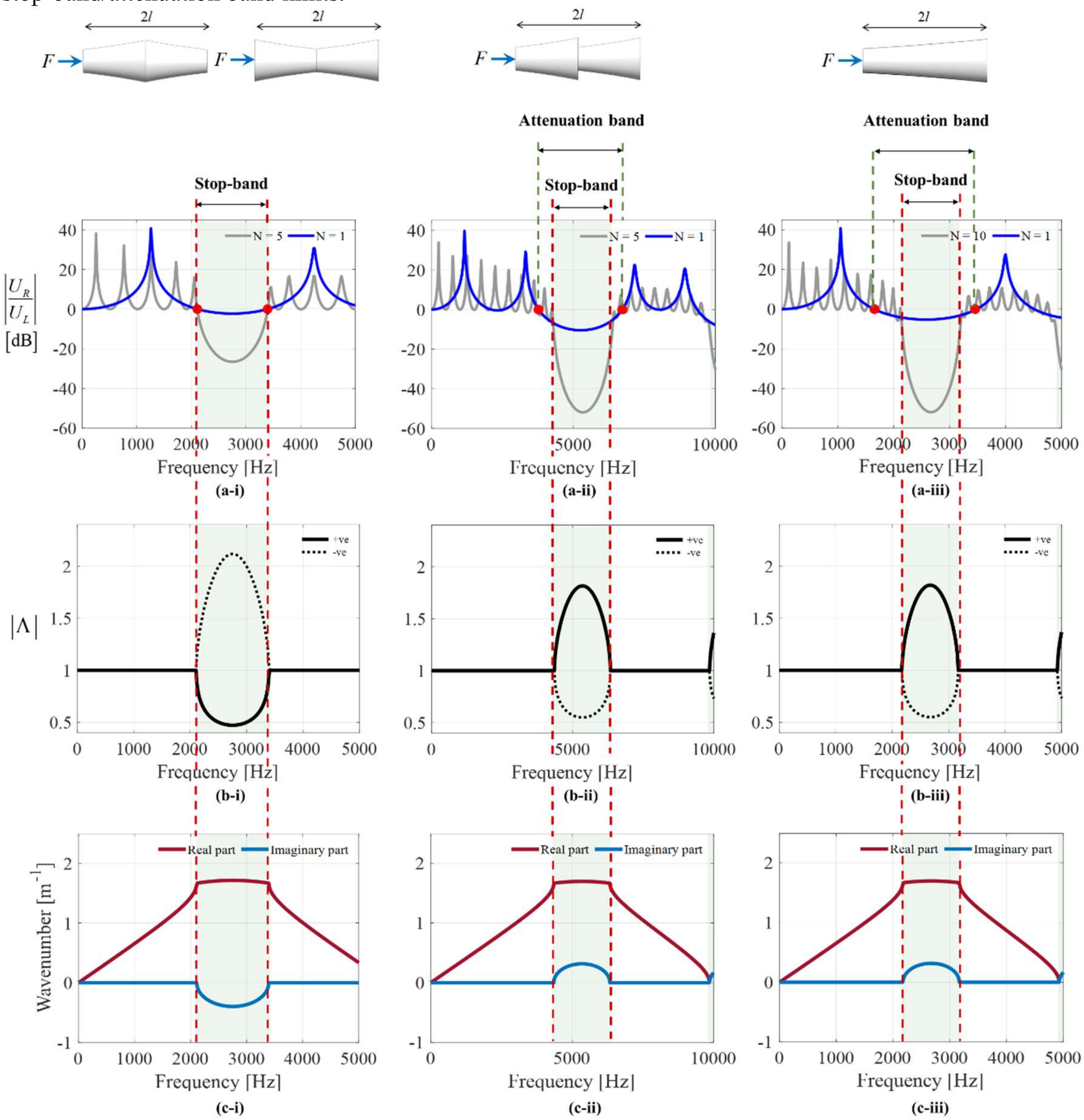

Source: Author own elaboration.

As can be observed in Figures C.1(ai–ci), the dispersion curve for symmetric structures corresponds to the stop-band predicted by the displacement transmissibility curve. However, in the case of asymmetric structures, shown in Figure C.1 (aii–ciii), a certain number of cells is required to reach the lower and upper limits of the stop-band of the infinite structure. This is because the greater the number of cells, the closer the structure will behave to an infinite one.

APPENDIX D – Experimental Modal Analysis (EMA)

This appendix describes the Experimental Modal Analysis (EMA) performed in symmetric and asymmetric cells. The experimental analysis was conducted as a complementary approach to investigating the dynamic behavior of the cells.

In the experimental procedure, the conical-shaped rods previously used in experimental setups were utilized in both symmetric and asymmetric configurations. The roving excitation method was employed. In this approach, the accelerometer (model PCB 352A24) with a nominal sensitivity of 100 mV/g was fixed at the center of the left end (point 17), as illustrated in Figure 42, while the impact hammer (model PCB 086E80) with a nominal sensitivity of 22.5 mV/N was moved to excite the structure at all the nodes indicated in Figure D.1. For each excitation point, an average of five frequency response measurements were performed. The signals were acquired and processed using a Dewesoft-Sirius system connected to a laptop.

Figure D.1 - Schematic representation of the roving excitation method, highlighting the nodes excited in the structure and the accelerometer positioned at the left end of a cell (point 17). Additionally, two photographs are provided showcasing the symmetric and asymmetric cells used in the experiments.

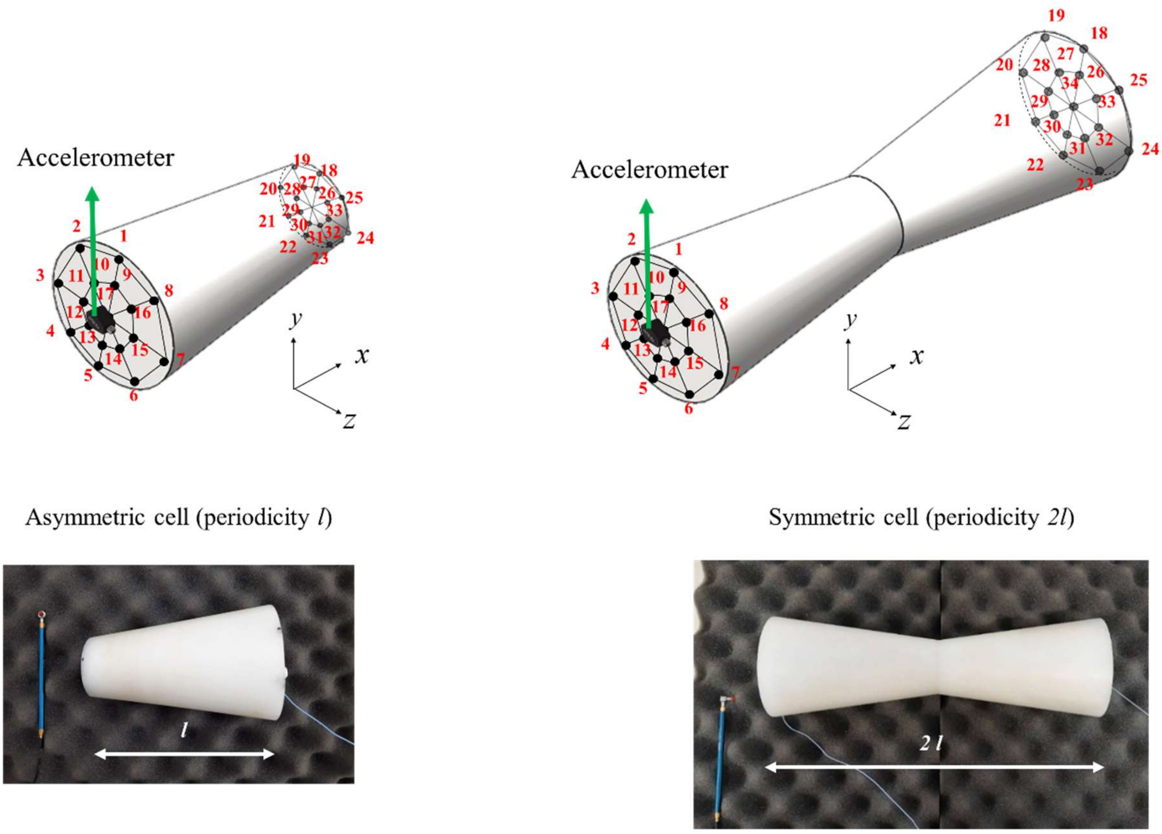

Source: Author own elaboration.

Signal processing was performed to extract and analyze the dynamic characteristics of the cells. The Complex Mode Indicator Function (CMIF) was computed as part of this process. CMIF is a method that provides a function for each reference degree of freedom (DOF), included in the analysis, using a poly-reference approach. This technique helps identify closely coupled modes and repeated roots by applying Singular Value Decomposition (SVD) to all measured Frequency Response Functions (FRFs). Peaks in the CMIF functions correspond to resonances, indicating the poles of the system under test (ALLEMANG; BROWN, 2006).

During data acquisition, the CMIF overlaid on the stabilization diagram to provide a comprehensive overview of the detected modes. Once the modes were identified, the autoMAC (Modal Assurance Criterion) was used to validate the distinction and accuracy of the estimated modes. The autoMAC evaluates the correlation between pairs of modes to ensure they are distinguishable based on the measured DOFs and FRFs. It produces values ranging from 0 to 1, where a value of 1 indicates perfect correlation (KHOO *et al.*, 2020).

Figure D.2 presents the CMIF and mode shapes obtained from the experimental modal analysis for the asymmetric cell. Table D.1 shows the AutoMAC values for the correlation of each mode with itself.

Table D.1 - AutoMAC between modes to itself (asymmetric cell).

Frequency [Hz]	**3344.52**	**5890.58**
3344.52	1	0.0522
5890.58	0.0523	1

Source: Author own elaboration.

.

Figure D.2 - Complex Mode Indicator Function (CMIF) and mode shapes of the asymmetric cell.

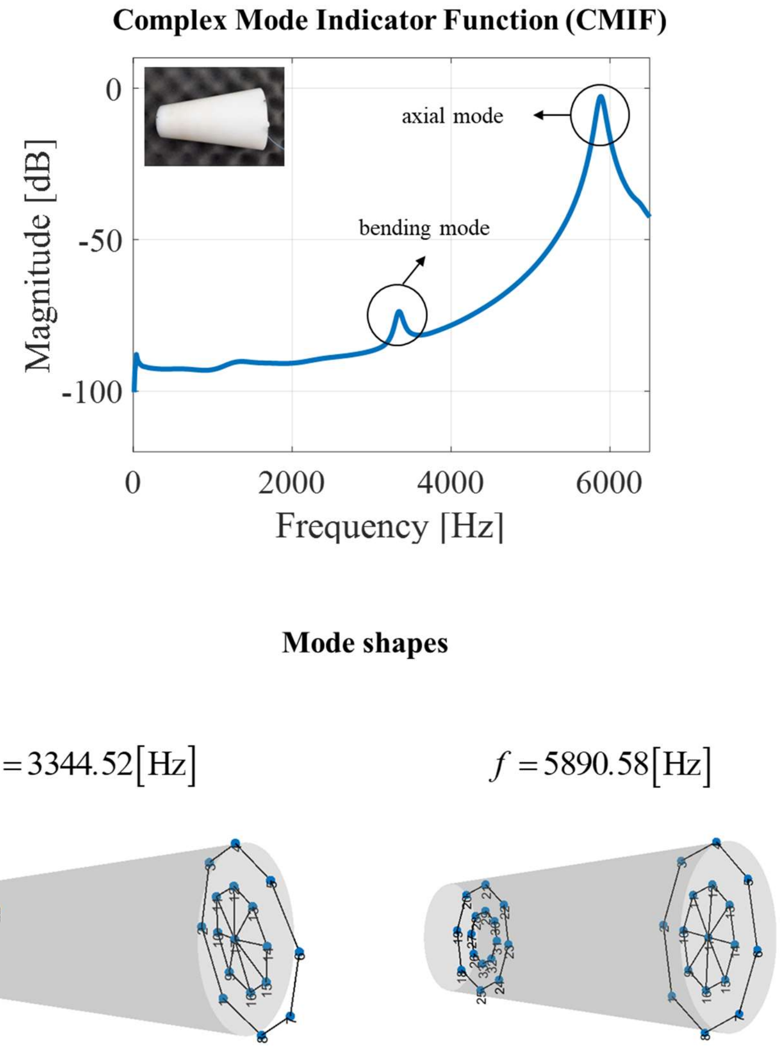

Source: Author own elaboration.

Figure D.3 presents the CMIF and mode shapes obtained from the experimental modal analysis for the symmetric cell and the Table D.2 shows the AutoMAC values for the correlation of each mode with itself.

Table D.2 - AutoMAC between modes to itself (symmetric cell).

Frequency [Hz]	**613.08**	**2079.86**	**3700.14**	**5802.21**
613.08	1	0.9110	0.1175	0.0191
2079.86	0.9110	1	0.0180	0.0062
3700.14	0.1175	0.018	1	0.0019
5802.21	0.0191	0.0062	0.0019	1

Source: Author own elaboration.

Figure D.3 - Complex Mode Indicator Function (CMIF) and mode shapes of the symmetric cell.

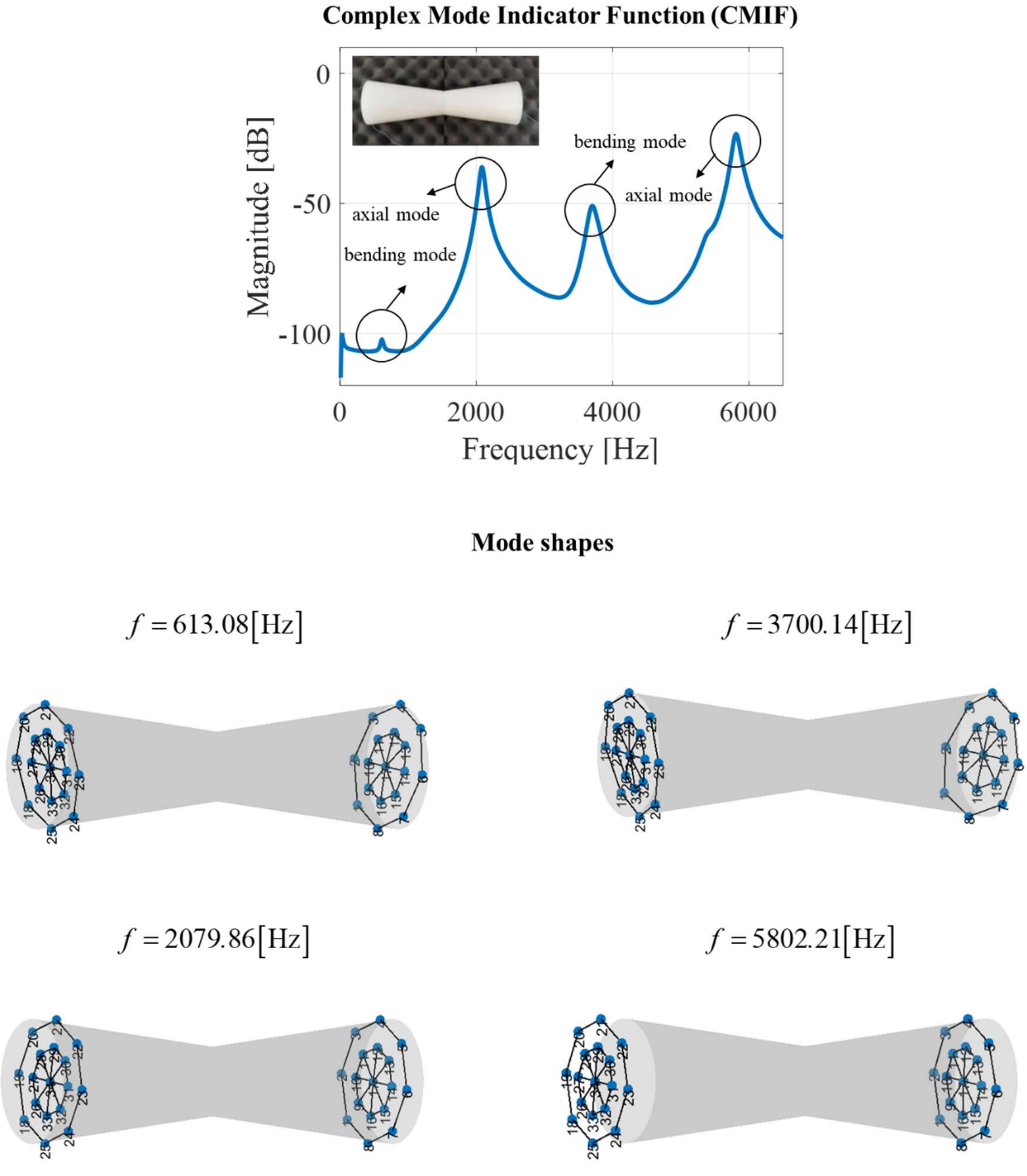

Source: Author own elaboration.

It can be observed that the modes obtained for both cells include not only the axial modes predicted by the theoretical predictions described in this thesis but also modes associated with flexural vibrations. The stop/attenuation band phenomenon discussed in this thesis is based solely on longitudinal displacement, excluding transverse displacement caused by Poisson's ratio effects (BANERJEE; ANANTHAPUVIRAJAH; PAPKOV, 2020) and flexural vibrations. These effects, which generally become significant at higher frequencies, can be analyzed using the Rayleigh-Love model (HAN *et al.*, 2014).

While these effects may have been present in the measurements discussed in Chapter 6 , their influence did not significantly affect the predicted attenuation bands or the minimum transmissibility. The additional effects observed in the experimental responses are primarily related to peaks associated with flexural vibrations.